https://doi.org/10.5194/essd-2024-299
Preprint. Discussion started: 29 August 2024

Open Access Earth System Science Data Discussions

A China dataset of soil properties for land surface modeling (version 2)

Gaosong Shi[1], Wenye Sun[1], Wei Shangguan[1,*], Zhongwang Wei[1], Hua Yuan[1], Ye Zhang[1], Hongbin Liang[1], Lu Li[1], Xiaolin Sun[2], Danxi Li[1], Feini Huang[1], Qingliang Li[1,3], and Yongjiu Dai[1]

[1]Southern Marine Science and Engineering Guangdong Laboratory (Zhuhai), Guangdong Province Key Laboratory for Climate Change and Natural Disaster Studies, School of Atmospheric Sciences, Sun Yat-sen University, Guangzhou 510275, China;
[2]School of Geography and Planning, Sun Yat-sen University, Guangzhou 510275, China;
[3]College of Computer Science and Technology, Changchun Normal University, Changchun 130032, China

Correspondence to: Wei Shangguan (Email: shgwei@mail.sysu.edu.cn)

Abstract. Accurate and high-resolution spatial soil information is crucial for efficient and sustainable land use, management, and conservation. Since the establishment of digital soil mapping (DSM) and the GlobalSoilMap working group, significant advances have been made in spatial soil information globally. However, accurately predicting soil variation over large and complex areas with limited samples remains a challenge, especially for China, which has diverse soil landscapes. To address this challenge, we utilized 11,209 representative multi-source legacy soil profiles (including the Second National Soil Survey of China, World Soil Information Service, First National Soil Survey of China, and regional databases) and high-resolution soil-forming environment characterization. Using advanced Quantile Regression Forest algorithms and a high-performance parallel computing strategy, we developed comprehensive maps of 23 soil physical, chemical and fertility properties at six standard depth layers from 0 to 2 meters in China with a 90 m spatial resolution (China dataset of soil properties for land surface modeling version 2, CSDLv2). Data-splitting and independent samples validation strategies were employed to evaluate the accuracy of the predicted maps quality. The results showed that the predicted maps were significantly more accurate and detailed compared to traditional soil type linkage methods (i.e., CSDLv1, the first version of the dataset), SoilGrids 2.0, and HWSD 2.0 products, effectively representing the spatial variation of soil properties across China. The prediction accuracy of most soil properties at the 0-5 cm depth interval ranged from good to moderate, with Model Efficiency Coefficients for most soil properties ranging from 0.75 to 0.32 during data-splitting validation and from 0.88 to 0.25 during independent sample validation. The wide range between the 5% lower and 95% upper prediction limits may indicate substantial room for improvement in current predictions. The relative importance of environmental covariates in predictions varied with soil properties and depth, indicating the complexity of interactions among multiple factors in the soil formation processes. As the soil profiles used in this study mainly originate from the Second National Soil Survey of China during 1970s and 1980s, they could provide new perspectives of soil changes together with existing maps based on 2010s soil profiles. The findings make important contributions to the GlobalSoilMap project and can also be used for regional Earth system modeling and land surface modeling to better represent the role of soil in hydrological and biogeochemical cycles in China. This dataset is freely available and can be accessed at https://doi.org/10.11888/Terre.tpdc.301235 (Shi et al, 2024).

1 Introduction

Soil plays a pivotal role in earth's systems, facilitating the cycling of water, energy, and carbon across varying temporal and spatial scales. Its significance lies in regulating ecosystems by providing vital nutrients to living organisms, storing and cycling water, heat, carbon, and essential nutrients, and serving as a medium for vegetation growth and structural support (Chaney et al., 2019; Crow et al., 2012). Soil data are essential for land surface models (LSMs), which form a part of Earth system models (ESMs) (Dai et al., 2019b; Luo et al., 2016). The diverse range of soil properties and their precise representation are crucial for robust land surface modeling, influencing various environmental, agricultural, and ecological assessments. There is an urgent need for detailed, accurate, and up-to-date soil information to develop solutions for these challenges and to inform decision-making related to natural resource management (Dai et al., 2019b).

In recent years, the national and global maps of soil properties have gained significant traction in research (Arrouays et al., 2017), with a surge of studies focusing on mapping one or more soil properties at high resolutions such as 90 meters spanning various countries. These include large-scale endeavors in Australia (Grundy et al., 2015; Viscarra Rossel et al., 2015), France (Chen et al., 2023; Mulder et al., 2016), Chile (Dinamarca et al., 2023; Padarian et al., 2017), Japan (Yamashita et al., 2024) and the United States (Ramcharan et al., 2018; Thompson et al., 2020). Chaney et al., (2019) even developed 30 m probabilistic maps of soil properties across the United States. Denmark has also developed national maps of soil texture at a finer 30 m resolution (Adhikari et al., 2013). Additionally, broader-scale resolution maps, ranging from 250 to 5000 m, have also been investigated at the national level, exemplified by Brazil's (Gomes et al., 2019), and expanded to continental scales including Africa (Hengl et al., 2015, 2021) and Europe (Heuvelink et al., 2016), and ultimately to global levels such as Global Soil Dataset for use in Earth system models (GSDE, Shangguan et al., 2014), Harmonized World Soil Database version 2.0 (HWSD 2.0, FAO & IIASA, 2023), SoilGrids 2.0, (Poggio et al., 2021).

Shangguan et al., (2013) pioneered the development of a comprehensive soil characteristics dataset specifically designed for land surface modeling over China (i.e., China Soil Dataset for Land Surface Modelling, CSDL, the first version dataset of this study). This dataset, based on 8,979 legacy soil profiles and the soil map of China (1:1,000,000), employs the conventional polygon linkage method (Batjes, 1995, 2002; Shangguan et al., 2012) to develop soil physical properties, chemical properties and fertility. It provides a spatial resolution of 30 arc-second (about 1 km at equator) and includes over 20 properties at 8 vertical soil depths (Shangguan et al., 2013). The dataset has been successfully applied in various fields. Despite its significant contributions to regional land surface modeling and geoscientific research, over time, several issues and shortcomings have been identified. First, while the dataset utilized soil profiles solely from the Second National Soil Survey of China (1979-1985), there is now a broader array of available soil profiles, including those from the World Soil Information Service (WoSIS, (Batjes et al., 2020)), regional database (Shangguan et al., 2012) and the First National Soil Survey of China (National Soil Survey Office, 1964). The integration of these soil profiles promises to substantially enhance the spatial representation and coverage of the dataset. Second, this dataset relies on the traditional polygon linkage method based on soil transformation rules (Shangguan et al., 2013, 2014), where results heavily depend on the accuracy of soil classification maps and are estimated as the average of a soil class or polygon, leading to discontinuous spatial estimates. The emergence of digital soil mapping (DSM) techniques (Mcbratney et al., 2003), particularly the success of machine learning in large-scale spatial prediction (Hengl et al., 2017; Poggio et al., 2021; Yan et al., 2020), presents a methodological advancement for this study. Recent studies indicate that advanced machine learning models often outperform simpler ones, with the size of the sample also emerging as a crucial factor influencing model performance (Padarian et al., 2020). Considering these advancements and the recognition of limitations in the existing dataset, there is a compelling rationale for pursuing a new version that addresses these challenges leveraging more soil profiles and contemporary mapping technologies.

For China, mapping datasets encompassing one or multiple soil properties have already been developed. Liang et al., (2019) and Chen et al., (2019) both developed high-resolution grid maps across China based on about 5,000 legacy soil profiles collected from the Second National Soil Survey of China, providing more detailed information for areas with spatial heterogeneity. However, Liang et al. (2019) focused solely on spatial estimates for soil organic carbon in the topsoil (0-20cm layer), while Chen et al. (2019) concentrated solely on spatial estimates for soil pH in the same layer. Both studies lack estimations for other soil property variables and deeper soil layers. Approximately 4,000 legacy soil profiles were utilized by (Zhou et al., 2019a) to develop a high-resolution national-scale dataset for total nitrogen in the topsoil (0-20 cm layer) with a 90 m resolution using machine learning methods. Similarly, Song et al., (2020) used over 5,000 soil profiles from the 2010s to produce high-resolution maps of soil organic carbon at six standard depths (0-5, 5-15, 15-30, 30-60, 60-100, and 100-200 cm) across China, achieving explained variances ranging from 0.16 to 0.57. Besides, Liu et al., (2022a) also employed machine learning methods to develop China's inaugural high-resolution national soil information grid dataset at a 90-meter resolution, utilizing soil samples from the most recent national soil specie survey (2009-2019). This dataset has significantly contributed to soil management, agricultural production, hydrological modeling, ecological development, and climate change mitigation. However, the study solely relied on a constrained set of about 4,500 soil profiles collected during the recent national soil survey, generating national grid maps for only some fundamental soil properties. The limitations stem from the absence of more comprehensive national grid maps for soil properties, such as Available phosphorous (AP), Available potassium (AK), Alkali-hydrolysable nitrogen (AN), porosity, and others, imposing constraints on applications that necessitate a broader spectrum of soil properties information. Additionally, there are abundant legacy soil profiles stored in global or regional databases (e.g., WoSIS, (Batjes et al., 2020)). These legacy soil profiles serve as a primary data source for digital soil mapping (Lagacherie et al., 2024; Song et al., 2020; Yang et al., 2022). For China, the Second National Soil Survey serves as a significant source of legacy soil profiles, offering valuable insights into soil properties and characteristics (Shangguan et al., 2013). Therefore, these rich legacy soil profile data should be fully utilized, as they better reflect historical mapping results, providing a new perspective for studying temporal changes in soil properties (Song et al., 2020).

This paper aims to develop a new version of CSDL (CSDLv2), with comprehensive soil physical properties, chemical properties for China at a 90 m resolution. This work builds on its previous version (hereafter referred as CSDLv1, Shangguan et al., 2013), integrating advanced machine learning algorithms, multi-source soil profile samples, and various high-resolution environmental covariates related to soil formation. Specifically, the novelty of the second edition dataset developed in this study, compared to the first edition, is manifested in the following aspects:

1. integration of multi-source soil profile samples, including soil profiles from the Second National Soil Survey of China (Shangguan et al., 2013), the World Soil Information Service (Batjes et al., 2020), the First National Soil Survey of China

(National Soil Survey Office, 1964), and regional databases (Shangguan et al., 2012), enhancing the spatial representation of soil profiles, instead of only data from the Second National Soil Survey of China in CSDLv1;

2. application of up-to-date machine learning methods, replacing conventional soil polygon linkage method;
3. accuracy improvement and enhanced resolution from the original 1 km to 90 meters; and
4. quantification of prediction uncertainty using Quantile Regression Forests (Meinshausen, 2006) instead of quality control information without explicitly uncertainty estimates in CSDLv1.

Additionally, the novelty of the second edition dataset compared to existing datasets lies in two main aspects: on one hand, a larger number of soil profiles were utilized in this study; on the other hand, this study developed over 20 comprehensive soil property variables, while most current research focuses on mapping a few basic soil properties.

2 Materials and Methods

The workflow of this study is shown in Fig. 1. Four main processes are involved in this framework:

1. Incorporating *in-situ* values of multiple soil profiles and overlaying them with covariates to generate a regression matrix for modeling
2. Using cross-validation to obtain optimal modeling parameters
3. Fitting prediction models based on the regression matrix
4. Applying spatial prediction models using high-resolution covariates and comparing predictions with existing maps using data-splitting and independent samples validation.

2.1 Study area and soil profiles

2.1.1 Study area

China, located in East Asia along the west coast of the Pacific Ocean, extends from 73°33' to 135°05' E longitude and from 3°51' to 53°33' N latitude, covering an east-west distance of about 5,000 km and featuring a continental coastline exceeding 18,000 km. The terrain of China exhibits a distinctive "ladder" pattern, with higher elevations in the west descending to lower elevations in the east. Mountains, plateaus, and hills comprise about 67% of the land area, while basins and plains make up the remaining 33% (Qin et al., 2016). China's topography is highly complex, encompassing an array of landforms such as extensive mountain ranges, vast plateaus, fertile plains, and deep basins. This diverse landscape is further complicated by a range of climatic zones determined by variations in temperature, precipitation, and altitude. These zones include temperate, subtropical, and tropical climates, with the temperate zone being the largest (Fan et al., 2016). Given the complexity and diversity of China's geographical and climatic conditions, the study of soil properties mapping across this vast nation is of paramount importance.

2.1.2 Soil profiles

Typical soil profiles representing main soil-landscapes were collected from four data sources: Second National Soil Survey of China (SNSSC, (National Soil Survey Office, 1996)), World Soil Information Service (WoSIS, (Batjes et al., 2020)), regional datasets (Shangguan et al., 2012), and First National Soil Survey of China (FNSSC, (National Soil Survey Office, 1964)). A total of 11,209 soil profiles were gathered, with distribution details as follows: 8,979 from SNSSC, 1,540 from WoSIS database, 614 from regional datasets, and 76 from FNSSC. Their spatial distribution is illustrated in Fig. 1, with different colors representing each data source. The soil property variables considered in this study are listed in Table 1. SNSSC, conducted primarily between 1979 and 1985, provided the majority of soil profiles, although coordinates were approximated due to GPS limitations at the time, impacting mapping accuracy (Lagacherie et al., 2024). Shi et al. (2024) improved the location accuracy of soil profiles in SNSSC by aligning detailed profile descriptions with environmental covariates. WoSIS, managed by the International Soil Reference and Information Centre (ISRIC), is a comprehensive global database that consolidates soil profile data from various sources under a common standard (Batjes et al., 2020). These data are standardized and harmonized to facilitate global soil research and enhance the accuracy of digital soil mapping efforts. It is worth noting that WoSIS contains soil profiles from the SNSSC. The following approach was employed to determine and eliminate potentially duplicate soil profiles in the WoSIS database that may overlap with those in the SNSSC: soil profiles were considered duplicates if they had identical depths of soil horizons or included at least three identical depths, exhibited similar soil property values, and had close geographic coordinates (latitude and longitude). Consequently, 101 duplicate soil profiles were removed from the WoSIS database, leaving 1,540 soil profiles for this study. The regional dataset was collected from five areas in 2008 and 2009 (Shangguan et al., 2012). FNSSC, initiated in 1958, laid the foundation for China's soil science database and agricultural soil classification. The probability density distribution of topsoil (0-5 cm) properties from different data sources is provided in Fig. S1. To align with international soil mapping standards, a continuous depth function using equal-area splines was applied to horizon data, defining six standard layers (0-5, 5-15, 15-30, 30-60, 60-100, and 100-200 cm). Detailed descriptions of the equal-area splines can be found in Bishop et al. (1999) and Liu et al. (2022a).

2.2 Environmental covariates

Following the *SCORPAN* (soil, climate, organisms, topography, parent material, age and space) concept (Mcbratney et al., 2003), over 150 environmental covariates associated with soil formation were collected to investigate the spatial distribution of soil properties for this work. A summary of some high-resolution covariates was provided in Table 2, while the complete list can be found in Table S1. These environmental covariates offer information on the factors related to soil properties.

Relief covariates primarily were derived from the MERIT Digital Elevation Model (DEM) dataset (https://hydro.iis.u-tokyo.ac.jp/~yamadai/MERIT_DEM/), a high-precision global DEM with a resolution of 3 arc-seconds (~90 m at the equator), vertically referenced to the EGM96 geoid and horizontally referenced to the World Geodetic System 1984 (Yamazaki et al., 2019). This dataset serves as an improved spaceborne DEM that significantly reduces the major error components found in other DEMs such as NASA's SRTM3 DEM, and Viewfinder Panoramas DEM (Li et al., 2023). Based on this DEM, other relief covariates such as slope, aspect, plan curvature, profile curvature, and terrain wetness index were calculated using SAGA GIS (Conrad et al., 2015).

Organism covariates were primarily sourced from six datasets: The Landsat 8 Collection 2 Level 2 (LC08C02), MODIS, GLOBELLAND30, the Global Accessibility Map, and GlobCover. L8C2L2 is an advanced satellite data product released by the United States Geological Survey (USGS). Landsat 8, part of the Landsat satellite series, is specifically designed for Earth observation and monitoring. Collection 2 represents an updated version of Landsat data products, incorporating various improvements and enhancements. High-resolution data such as NDVI, NDWI, Band 5, and Band 7 with 90m spatial resolution were obtained from this database via the Google Earth Engine (GEE) platform. MODIS data offers an efficient method for monitoring biosphere changes and understanding Earth's climate system, available at a spatial resolution of 1 km. GLOBELLAND30, a significant achievement from China's global and local land cover remote sensing mapping and technology research project, provides comprehensive global land surface coverage at a 30 m resolution. The Global Accessibility Map illustrates urban and rural population gradients at a 1 km resolution over the years 2000 to present. Developed by the European Space Agency, the GlobCover dataset provides a global land cover map at a 1 km resolution.

Climate factors were chiefly obtained from the MODIS, WorldClim, and CHELSA-climate datasets (DAAC, 2018; Karger et al., 2020), primarily offering at a 1 km spatial resolution and covering the years 1970-2000. Soil factors, i.e., soil classifications, were mainly derived from the Harmonized World Soil Database also available at a 1 km spatial resolution (Nachtergaele et al., 2012). Parent material factors were represented by the depth to bedrock maps and a lithological map (Yan et al., 2020).

All environmental covariates were reprojected to a unified coordinate reference system, specifically Goode’s homolosine projection applied to the World Geodetic System (WGS) 1984 projection. This projection was chosen as it is the most effective at minimizing distortions over land among the equal-area projections available in open-source software (Moreira De Sousa et al., 2019). Additionally, the nearest interpolation and bilinear interpolation algorithms were applied to the subtype data (e.g., vegetation type) and continuous variables, respectively, to resample these environmental covariates to a raster cell size of 90 m resolution for spatial modeling and map prediction.

Considering the substantial number of available environmental covariates, those with an absolute Pearson correlation coefficient of less than 0.05 with the target variable were excluded. Subsequently, redundant covariates with a Pearson correlation coefficient greater than 0.8 with any other covariate were removed to eliminate autocorrelation among them. For each pair of environmental covariates with a correlation exceeding this threshold, only the first one in alphabetical order was retained for the modeling phase (Poggio et al., 2021). This process reduced the initial number of environmental covariates to approximately 80 layers.

In this study, the Recursive Feature Elimination (RFE) method was implemented using the *sklearn.feature_selection* package in Python, which offers a balanced approach between accuracy and computational efficiency. RFE is a robust technique, widely recognized for its efficacy in selecting optimal covariate sets for regression tree models (Gomes et al., 2019). The RFE process begins by fitting a model that includes all environmental factors, evaluating its performance, and ranking the covariates based on their importance. The least significant factors are systematically eliminated, followed by re-fitting the model and reassessing performance. This iterative procedure continues until the pool is reduced to a set between zero and the total number of environmental covariates. This method relies on out-of-bag (OOB) cross-validation, making it a reliable selection approach for models such as random forests, even though it does not test every possible combination of covariates (Nussbaum et al., 2018). The RFE process is independently conducted on each subset, leveraging the default hyperparameters of the random forest algorithm as provided by the *RandomForestRegressor* package in Python. The optimal subset of variables is identified when further iterations no longer yield improvements in model performance, defined by the minimization of the loss function. For this study, the OOB root-mean-square error (RMSE) was used as the loss function. The ultimate set of covariates was identified as the combination that minimized the loss function. The aforementioned analysis was executed for all target variables and depths. For instance, with surface (0-5 cm) soil organic carbon, 35 environmental covariates remained for analysis after the filtering process (Fig. 3), and marked with a superscript "1" in Table S1.

2.3 Digital soil mapping

2.3.1 Spatial prediction and uncertainty

The Quantile Regression Forest (QRF) model was employed to evaluate the statistical relationship between each soil property at six layers and environmental covariates. The QRF algorithm, introduced by Meinshausen, (2006), is an ensemble machine learning model that utilizes tree structures and bootstrapping techniques to create a collection of tree models. Each tree is developed from a learning set generated by repeatedly sampling calibration samples through bootstrapping, with node splits influenced by a randomly selected subset of covariates. The final prediction value at each predetermined quantile is obtained by averaging the predicted values from all trees. Building on the foundation of Random Forests (RF, (Breiman, 2001)), QRF algorithm present a novel approach to enhancing regression tree performance (Koenker, 2005). In RF, averaging across multiple tree-based models results in more accurate predictions compared to using a single regression tree. The QRF not only provides a precise approximation of the conditional mean $E(Y|X = x)$, but it also offers insights into the full conditional distribution of the dependent variable. Consequently, conditional quantiles can be inferred using QRF algorithm, which is a generalization of RF. The conditional distribution of Y given $X = x$ is defined as $F(y|X = x) = P(Y \leq y|X = x)$. To estimate $F(y|X = x)$, a weighted empirical cumulative distribution function is considered:

$$\hat{F}(y|X = x) = \sum_{i=1}^{n} w_i(x, \theta) Y_{\{Y \leq y\}} \tag{1}$$

The tree-based model developed using QRF algorithm follows the RF methodology. However, unlike RF, where only the mean of the observations within each node is retained, the QRF approach preserves the values of all observations within each node. This comprehensive set of observations in each node is utilized to derive the quantiles, which are subsequently used to construct prediction intervals. These intervals serve as a measure of the prediction uncertainty, providing a more detailed understanding of the conditional distribution of the target variable. Additionally, the uncertainty estimates evaluated by QRF are likely more accurate and interpretable than those derived from regression kriging, particularly in areas with sparse samples (Liu et al., 2022a). Furthermore, QRF is capable of handling complex non-linear relationships and multivariate interactions, offering high predictive power (Gyamerah et al., 2020). This distinguishing advantage sets QRF apart from other machine learning algorithms (Liu et al., 2022b).

The selection of hyper-parameters, specifically the number of randomly selected variables from all predictors (*max_features*) and the minimum node size (*min_samples_leaf*), plays a crucial role in determining the performance of the RF model. These hyper-parameters significantly influence the model's predictive accuracy. Other parameters, such as the number of trees (*n_estimators*), were not optimized during the RF's training process. To address potential overfitting concerns, the values of *max_features* and *min_samples_leaf* were fine-tuned using a 10-fold cross-validation method. This approach involved randomly dividing the entire dataset into ten folds. One-tenth of these sub-datasets was utilized as the validation sample, while the remaining sub-datasets were applied for training the QRF model. This tuning was conducted using the gridded direct search approach, with *max_features* explored within the range of [1, 30] at single intervals, and *min_samples_leaf* within the range of [5, 30] at intervals of five. In this study, the aforementioned hyperparameter search was conducted for each of the six soil depth layers for every soil property. These hyperparameters were then used for modeling and spatial prediction of the corresponding soil property variables at their respective depths. To maintain brevity, Table S2 presents the tuned model hyper-parameters for each soil property considered at the 0-5 cm depth interval.

The relative importance of covariates in the trained QRF model was assessed to investigate the impact of environmental factors on spatial variations of soil properties. This importance was determined by evaluating the influence of each covariate on the model's prediction performance. The relative importance of each covariate was quantified using the increase in mean square error (%IncMSE), a metric derived from permuting the values of a covariate to remove its information content. By comparing the model's accuracy before and after permutation, it was possible to determine how crucial each covariate was in predicting soil properties. A higher %IncMSE indicated a greater importance of the covariate, signifying that its presence substantially contributed to the model's predictive accuracy. This relative importance allows for a detailed analysis of how different environmental factors control spatial variations in soil properties, providing valuable insights for digital soil mapping.

Mapping China, covers approximately 9.6 million km², at 90 m resolution requires more than 10^9 pixels for each soil property at each depth, posing a considerable challenge. Due to the extensive geographic coverage and high-resolution requirements in soil mapping for this study, predicting each soil property at a specific depth involves a substantial volume of data, with environmental covariates data reaching up to 470 GB. Faced with such extensive data processing demands, conventional single-machine resources often prove inadequate and challenging to cope with. Therefore, to overcome the memory limitations imposed by high-resolution mapping and enhance the computational efficiency of spatial prediction, we implemented parallel computing. Initially, we partitioned environmental covariates into distinct 1°×1° blocks. Using the finalized model, a single core performed spatial predictions within each block. Leveraging multiple cores processing, we simultaneously handled multiple blocks, significantly accelerating spatial predictions. Upon acquiring the outcomes for every block, we utilized image mosaicking to seamlessly integrate these outputs, ultimately assembling the comprehensive map of various soil properties and depths across China. All the experiments are performed on a Linux server with Intel Core (TM) i9-10980XE, 3.00GHz×64 CPU, 512 GB RAM (Random Access Memory) and two NVIDIA RTX A5000 graphics cards. All scripts were written in the open-source Python programming environment with Python version 3.11.4 (https://www.python.org/) using PyCharm with version 2024.3.28. The "RandomForestQuantileRegressor" package was employed for model construction. The optimization of the model was performed using "scikit-learn" library, while the "gdal" and "matplotlib" packages were utilized for data processing and visualization, respectively.

Using the selected environmental covariates from the aforementioned feature engineering, the constructed model was applied to compute four different values at every 90 m pixel across all standard depth layers (0-5, 5-15, 15-30, 30-60, 60-100, and 100-200 cm) specified by GlobalSoilMap (Arrouays et al., 2014) over China, capturing the conditional distribution: the mean, 0.05 quantile ($q_{0.05}$), median (0.50 quantile, $q_{0.50}$), and 0.95 quantile ($q_{0.95}$). The mean value was used to generate the national gridded soil maps, which constitutes the final soil properties dataset product. The calculated median, along with the 0.05 and 0.95 quantiles, was used to estimate uncertainty. Uncertainty was expressed as the upper and lower limits of a 90% prediction interval, represented by the empirical distribution's 0.05 and 0.95 quantiles, respectively. Furthermore, to facilitate comparison, the prediction interval relative to the median ($q_{0.50}$) was used as an indicator of uncertainty (Liang et al., 2019; Liu et al., 2022a). A higher ratio for a pixel indicates greater uncertainty in the predicted value for that location (Poggio et al., 2021).

2.3.2 Evaluation criteria

To validate the performance of QRF model for generating CSDLv2, two validation methods were employed to ensure that the CSDLv2 product has low errors in both spatial and vertical depth scales against *in-situ* values. The first method involved randomly selecting 10% of the multi-source soil profiles as test samples, while the remaining 90% were used for training the model (i.e., data-splitting). The second method took the WoSIS dataset as an external independent validation dataset, with the rest of the data used for model training (i.e., independent samples). Based on the training soil profiles, these two validation approaches were implemented to assess the accuracy performance of predictive mapping for each soil property at various depths. Three statistics, namely, Modelling Efficiency Coefficient (MEC, (Krause et al., 2005)), root mean square prediction error (RMSE), and mean prediction error (ME) were calculated to evaluate the models' predictive performance. They were calculated as follows:

$$MEC = 1 - \frac{\sum_{i=1}^{N}\left(z(s_i)-\hat{z}(s_i)\right)^2}{\sum_{i=1}^{N}(z(s_i)-\bar{z})^2}, \tag{2}$$

$$RMSE = \sqrt{\frac{1}{N}\sum_{i=1}^{N}\varepsilon(s_i)^2}, \tag{3}$$

$$ME = \frac{1}{N}\sum_{i=1}^{N}\varepsilon(s_i) \tag{4}$$

, where z represents the observed soil variable, $\hat{z}$ is the predicted soil variable at location s_i ($i = 1, \ldots, N$; $s_i \in \wp$), and N is the total number of population units in the study area $\wp$. Regard the prediction error as the difference between the observed (z) and predicted ($\hat{z}$) values of a soil property at the i^{th} spatial location, denoted by $\varepsilon(s_i) = z(s_i) - \hat{z}(s_i)$. To guarantee the accuracy and reliability of our results, we performed 20 repetitions of 10-fold cross-validation and calculated the mean and standard deviation of the measurements.

The soil property maps predicted in this study were compared to three existing soil map datasets. The first dataset is SoilGrids 2.0, accessible at https://soilgrids.org/, which has a 250-m resolution (Poggio et al., 2021). It represents an advancement over previous global soil properties maps, known as SoilGrids250m (Hengl et al., 2017), incorporating the up-to-date machine learning methods and benefiting from the expanded availability of standardized soil profile data worldwide, along with environmental covariates (Poggio et al., 2021). The second dataset is CSDLv1 with a resolution of 1 km (Shangguan et al., 2013), accessible at http://globalchange.bnu.edu.cn. Lastly, we considered the Harmonized World Soil Database v2.0 (HWSD 2.0), known for its soil property maps created via a soil type linkage method, available at https://www.fao.org/soils-portal/data-hub/soil-maps-and-databases/harmonized-world-soil-database-v20/en/. The HWSD 2.0 has been synthesized by integrating regional and national soil data globally (FAO & IIASA, 2023). To quantify the enhancement of our predictions over existing soil maps, we calculated the relative improvement (RI) using both MEC and RMSE metrics, employing the following equations:

$$RI_{MEC} = \frac{MEC_{CSDLv2} - MEC_{existing}}{MEC_{existing}} \tag{5}$$

$$RI_{RMSE} = \frac{RMSE_{existing} - RMSE_{CSDLv2}}{RMSE_{existing}} \tag{6}$$

, where RI_{MEC} and RI_{RMSE} denote the relative improvement concerning MEC and $RMSE$, respectively. MEC_{new} and $RMSE_{new}$represent the accuracy statistics for predictions in this study, while $MEC_{existing}$ and $RMSE_{existing}$ signify the accuracy statistics for the existing soil maps. An $RI > 0$ denotes CSDLv2 outperforms the existing soil maps.

Considering the unavoidable impact of various error sources on any model for DSM, it is essential to quantify the associated mapping uncertainty (Yan et al., 2020). To evaluate uncertainty, the prediction interval coverage probability (PICP) was employed based on the randomly held-back soil profile test samples. PICP represents the proportion of observations at each depth encapsulated by the corresponding prediction interval (Li et al., 2023). In this study, the prediction interval was estimated using the aforementioned QRF model. If the uncertainty estimates are reasonably defined, the PICP should yield an estimate of 90% for a 90% (or 0.9) prediction interval. A PICP significantly greater than 0.9 suggests that the uncertainty has been underestimated, whereas a PICP significantly less than 0.9 indicates that it has been overestimated (Liu et al., 2020; Poggio et al., 2021).

3 Results

3.1 Statistical analysis

The probability density distributions of topsoil (0-5 cm) properties from different data sources are shown in Fig. S1, with different colors representing different data sources. If a color representing a data source is absent in some probability density distribution charts, it indicates that the soil property is not available from that data source. As observed in Fig. S1, the probability density distributions of soil properties from multiple sources exhibit a generally similar trend, with minor differences that enhance the representativeness of the soil profile samples. The abundance of soil profile data allows for a more detailed characterization of spatial variations in soil properties, particularly in a large and topographically diverse country like China (Liu et al., 2022a). Descriptive statistical analyses of soil properties across six standard depths are presented in Table S3. For most soil property variables at multiple depths, there is an extensive amount of soil profile data. Different soil properties exhibit varying trends with depth, accompanied by a large range and variation (see coefficient of variation). Overall, the average concentrations of most soil property variables tend to decrease with increasing depth (e.g., OC, TN), showing positive skewness distributions. Regarding the homogeneity of variance, Levene's test yielded p-values greater than 0.05 between data from any soil property, indicating no statistically significant differences between samples from different depths.

3.2 Predictive performance

After training and optimization, the effectiveness of the QRF model was evaluated. Using the test set, the model's prediction accuracy across multiple depths was assessed under two validation methods: Table 3 and Table S4 presents the predictive performance using a data-splitting strategy, where 10% of aggregated soil profiles were randomly partitioned as the test set. This validation of CSDLv2 was compared with the validation of the three existing soil map datasets using all soil profiles in this study. Table S5 displays the model's performance when modeling soil profiles from remaining data sources, validated independently using WoSIS data.

Overall, model performance varied depending on soil properties. The mean ME values were nearly zero, indicating that the predictions were generally unbiased. Soil pH was predicted with the highest accuracy, with MEC performance ranging from 0.75 to 0.68 across depths in the data-splitting validation strategy. That is to say that more than 68% of the pH variation can be explained and the predicted values are in good agreement with the *in-situ* values. This result is consistent with previous studies (Chen et al., 2019; Hu et al., 2024; Lu et al., 2023). The mean MEC values for sand and clay content were slightly higher than those for silt content, indicating that sand and clay are slightly more predictable than silt. As soil depth increased, MEC values showed a decreasing trend, while RMSE values increased, indicating a vertical decline in the predictability of soil texture. This trend is similar to the findings of Liu et al., (2020). The model's predictive performance at the 5-15 cm depth interval was better than at the 0-5 cm depth interval, with higher MEC values and lower RMSE values. The prediction accuracy for OC was relatively high, with approximately 60% of the variation in soil surface (0-5 cm) OC explained in both data-splitting and independent validation methods. This performance surpasses the accuracy reported in related literature for OC prediction (Liang et al., 2019; Padarian et al., 2017). The prediction accuracy for soil properties content such as BD, gravel, TN, CEC, TK, and TP is higher at depths less than 30 cm. These models can explain 30% to 60% of the variation in these soil properties, with accuracy comparable to that reported in related studies (Mulder et al., 2016; Ramcharan et al., 2018).

The model's performance varied with soil depth. For most soil property variables, including OC, TN, and BD, predictive accuracy decreased significantly with increasing depth. In contrast, the accuracy for CEC, gravel content, and TK only slightly declined. This decrease in accuracy for deeper layers has been noted in previous studies on soil organic carbon prediction (Mulder et al., 2016; Padarian et al., 2017), primarily because most environmental covariates predominantly characterize surface conditions, leading to weaker correlations with deeper soil layers (Liu et al., 2020). Conversely, the prediction accuracy for soil pH value slightly improved with increasing depth. This may be partially attributed to the greater stability of these properties in subsurface layers at a broad scale, resulting in more stable responses to regional covariates (Liu et al., 2020). This observation aligns with the findings of Padarian et al., (2017). Additionally, independent samples validation is an effective approach to assess the validity of models and has been utilized in multiple studies (Lamichhane et al., 2019). Table S5 summarizes the model's predictive performance based on independent validation and compares it with other data products. These results also demonstrate the reliability of the predictive model.

3.3 Spatial patterns

Fig. 5 illustrates the maps of soil physical properties, chemical properties, and fertility at the soil surface (0-5 cm) over China at 90 m resolution. The spatial distribution of the complete soil properties (as listed in Table 1) can be found in the Fig S2-24. The gross pattern for all soil properties at multiple depths is clear.

As shown in Fig. 5(a), the pH values (H_2O) in the topsoil range from 4.3 to 9.8. Soils south of 30°N are predominantly acidic to strongly acidic, while those in the northern and northwestern regions are mostly basic or strongly basic. In some southern mountainous and northeastern forested areas, soils appear to be acidic (pH < 7.2). In certain northern regions, especially in desert areas, soils are alkaline (pH > 7.2). This distribution aligns with the common understanding that areas with low precipitation tend to have alkaline soils, whereas areas with high precipitation tend to have acidic soils.

For BD, as shown in Fig. 5(b). Overall, northern regions tend to have higher bulk density due to low organic matter content and frequent agricultural activities. Southern regions generally have lower bulk density owing to higher organic matter content and looser soil particles. Northwest arid regions exhibit high bulk density, while the Qinghai-Tibet Plateau has low bulk density. Southeastern coastal areas show significant variation in bulk density, heavily influenced by land use practices.

For OC, as shown in Fig. 5(c). The OC content decreases from southeast to northwest, corresponding with the influence of the southeast monsoon. The highest OC levels are found in the peatlands and forested areas of the southeastern Tibetan mountains and the forested regions of northeast China, where human activities are minimal. In contrast, lower OC values are observed in the northern and northwestern regions, particularly in the deserts. OC content is closely related to climatic conditions and land use practices (Zhang et al., 2023b; Zhou et al., 2019b). Areas with high precipitation and good vegetation cover have higher OC levels, while areas with low precipitation and poor vegetation cover have lower OC levels.

The mean predicted maps of soil texture (clay, silt, and sand contents) at different depths across China are shown in Fig 5(e)-(h), respectively. Overall, clay content was predicted to be low in the northern and northwestern regions, while higher in the southern regions. The lowest clay content was found in the deserts of the northwest, and the highest in the Yunnan-Guizhou Plateau. Relatively higher clay content was observed in some southern provinces such as Guangdong and Guangxi. Silt content was predicted to be high in the Loess Plateau and eastern China, while it was lower in the deserts of the northern and northwestern regions. These findings were consistent with previous studies (Liu et al., 2020). The predicted soil texture patterns fit well with the general characteristics and distribution of known Chinese soils (Gong et al., 2014).

For CEC, the spatial distribution of surface CEC is shown in Fig 5(j). CEC represents the total amount of exchangeable cations that soil can absorb, serving as a crucial indicator of soil fertility, nutrient retention capacity, and buffering capacity, thereby influencing plant growth. Lower CEC value indicate that the soil can store fewer nutrients. The CEC levels are closely related to soil type, climatic conditions, and land use practices (Beillouin et al., 2022). Generally, soils with higher clay and organic matter content have higher CEC values compared to those with sand or silt. Fig 5(j) indicates that higher surface soil CEC values are found in the Qinghai-Tibet Plateau and the peat and forest regions in the northeast (i.e., high-biomass or low-leaching areas). Lower CEC values are observed in the southeastern regions and the arid and semi-arid areas in the north, with the lowest CEC values found in desert areas. The relatively low CEC in the southeastern regions is attributed to higher temperatures and rainfall, leading to strong leaching loss of exchangeable substances.

The spatial distribution of TK, TP, and AK are shown in Fig.5(l), Fig.5(m), Fig.5(n), respectively. Sedimentary rocks in Southwest China are abundant in phosphorus, leading to relatively higher TP levels in soils derived from these rocks. In contrast, South China's soils typically exhibit lower TP levels due to extensive weathering and leaching. Alpine regions with significant organic matter accumulation are predicted to have relatively high TP content. The concentrations of both TK and AK diminish generally from north to south, despite their distribution patterns are rather different. Low levels of TK are found in tropical regions, whereas high levels are located in the Qinghai-Tibet Plateau and northeastern China. High values of AK are dispersed throughout western Tibetan Plateau. The spatial patterns of the variables of interest listed in Table 1 at multiple depths can be found in the supplementary materials. These spatial distributions are consistent with those reported in other similar studies (Hu et al., 2024; Liu et al., 2022a, Poggio et al., 2021).

3.4 Uncertainty

Table S6 lists the all PICP values for different soil properties at multiple depths, calculated based on randomly held-back test samples. For a 90% (or 0.9) confidence interval, 90% of the observations are expected to fall within the predicted lower and upper limits. It can be seen that the PICP values for all soil properties at six standard depths are very close to 90%, indicating that the predicted lower and upper limits estimated by the QRF method are appropriate. In other words, the uncertainty estimates are largely reliable. It was observed that different soil properties exhibit distinct spatial patterns of prediction uncertainty, but different depths of the same soil property show similar patterns. Fig. S25 shows the uncertainty maps for soil OC and pH predictions at 0-5 cm and 60-100 cm depths interval as examples. For OC, regions with relatively simple terrain, such as deserts, the North China Plain, and the Northeast Plain, exhibit lower uncertainty. In contrast, the central Qinghai-Tibet Plateau and western Inner Mongolia, where sampling is sparse and OC content is low, show higher uncertainty. The Altai region, with its complex terrain and diverse landscape types, also exhibits relatively high uncertainty. For soil pH, regions with high prediction uncertainty are found in Southwest China, where samples are sparse in complex soil landscapes.

3.5 Relative importance of predictors

The relative importance of environmental covariates for soil properties prediction at the 0-5 cm depth interval is shown in Fig. 6 and Fig. S26, displaying only the top 15 most important environmental covariates. Overall, organisms type accounts for a significant proportion among different categories of environmental factors. There are variations in the relative importance of environmental covariates across different soil property variables.

For soil pH, in the optimal QRF model, the climate factor (eg. MODCF) was identified as the most important variable, with an importance exceeding 30%, significantly higher than other covariates. The leaf area index (LAI) ranks second in relative importance. Previous studies have also indicated that LAI is a key factor in predicting soil pH (Sun et al., 2023). Other environmental covariates had relatively smaller contributions. In terms of covariates types, organisms factors accounted for 50% of the contribution to soil pH prediction, followed by relief factors (23.9%) and climate factors (17.4%).

For OC content, terrestrial ecosystems (TERECO) and climate factors (MODCF) are the most important covariates, followed by depth to bedrock and elevation (DEM). Shallow bedrock typically results in thinner soil layers, which limit soil development and the accumulation of organic carbon. In contrast, deeper bedrock allows for thicker soil layers, providing more space and time for OC accumulation. DEM can indirectly reflect differences in land use and vegetation types, which can also affect the distribution of OC content. This indicates that the prediction of soil organic carbon is influenced by multiple factors. Many studies have shown that organisms factors (e.g., landuse) is the most important predictor (Gomes et al., 2019).

For sand prediction, elevation and Mean Annual Cloud Frequency (MODCF) rank as the top two most important covariates in the QRF model. Altitude primarily affects soil through gravitational and erosional processes, which transport fine particles and leave behind coarse particles (Li et al., 2023). This is evident in the relatively higher sand content in most mountainous areas compared to adjacent lowland regions. Thermal processes drive physical weathering, while wind, water, and terrain govern erosion processes, predominantly shaping the distribution patterns of sand in China.

For silt prediction, climate-related factors (e.g., TNSMOD, MODCF, and wc2.1_srad) are the most important covariates. Apart from climate, terrain factors (e.g., DEM, DEM_vbf, and slope) also play crucial roles in silt prediction. Terrain features largely determine gravitational and hydraulic conditions, thereby influencing the erosion, redistribution, and sorting processes of soil particles. This observation is consistent with previous studies (Hengl et al., 2017), indicating that climate data can enhance the predictive performance of soil texture models.

For clay prediction, organic matter (e.g., TERECO) ranks as the most important environmental covariate, followed by climatic variable wc2.1_srad. Terrain-related variables (e.g., DEM, DEM_popn, and slope) rank second in importance overall, exerting their influence by controlling local moisture and thermal conditions, as well as redistributing terrain material (Liu et al., 2020). Other studies have similarly shown that vegetation indices, rock type, bioclimatic zones, and agricultural indices can help characterize changes in soil clay content (Ge et al., 2019; Hengl et al., 2017). It is worth noting that these discussions are unrelated to soil formation processes but rather assess changes in soil clay content. This may be because they overlap with parts of the soil clay profile, thus influencing their importance.

For CEC prediction, the most important covariate is terrestrial ecosystems (i.e. TERECO). Plant roots can alter the chemical environment of the soil by secreting organic acids and other substances, which influence the dissolution and reprecipitation processes of soil minerals. These changes can affect the soil's CEC. Shiri et al., (2017) have mainly discussed the relationships between soil carbon content and organic carbon, clay content, and particle size.

4 Discussion

4.1 Comparison with previous products

Table 3, S4 and S5 present the accuracy assessments of our predictions (i.e., CSDLv2), CSDLv1 (Shangguan et al., 2013), SoilGrid 2.0 (Poggio et al., 2021), and HWSD 2.0 (FAO & IIASA, 2023) at six standard depth intervals using data-splitting validation and independent sample validation methods, respectively. Table 3 lists the validation accuracy of selected soil properties using the data-splitting validation method, while Table S4 provides the complete accuracy assessments for all soil properties of interest. Table S5 identifies the variables for which the WoSIS database can serve as independent samples. Overall, our predictions, whether using data-splitting validation or independent sample validation, achieved relatively higher MEC values and lower RMSE values across multiple depths for most target variables, demonstrating much greater accuracy than existing soil property maps (FAO & IIASA, 2023; Poggio et al., 2021; Shangguan et al., 2013; Song et al., 2020; Zhou et al., 2019b). Specifically, using data-splitting validation as an example, our predictions for pH showed an improvement in MEC by 15%-19% and a reduction in RMSE by 11%-14% compared to SoilGrid 2.0. For other soil properties (OC, BD, TN, CEC), the prediction MEC improved by 11%-800% and RMSE reduced by 8%-78%. Compared to CSDLv1, our prediction performance for pH improved by 50%-162% in MEC and reduced by 31%-33% in RMSE, while for other soil properties (OC, BD, TN, CEC), the prediction MEC improved by 132%-840% and RMSE reduced by 17%-100%. Compared to HWSD 2.0, the prediction performance showed the greatest improvement in MEC and the most significant reduction in RMSE. The ME values indicated that SoilGrid 2.0 significantly overestimated TN content, whereas CSDLv1 and HWSD 2.0 underestimated it. Additionally, in the independent validation (Table S5), across predictions of various soil properties at different depths, this study demonstrates overall predictive performance that is comparable to or better than SoilGrid 2.0, even though SoilGrid 2.0 used all the soil profiles of WoSIS in its production. Moreover, it shows superior performance compared to CSDLv1 and HWSD 2.0.

Such a national-scale publication of soil maps hides most of the details. Nevertheless, because the soil properties are predicted at a 90 m resolution, portions of the maps can be enlarged to reveal increasingly detailed information up to the limit of that resolution. Using the example of surface (0-5 cm) OC content, Fig. 4 shows a visual comparison within a window in western Sichuan Province (102.92°-104.08°E and 30.92°-32.08°N). This window corresponds to the red window in Fig. 1. The comparison is between the dataset developed in this study (CSDLv2) and the widely used SoilGrid 2.0, CSDLv1, and HWSD 2.0. The OC map produced in this study clearly reveals spatial variability with local morphology and provides more detailed information than the other three maps. Moreover, the CSDLv2 and SoilGrid 2.0 datasets, both products of advanced digital soil mapping techniques, exhibit notably higher OC content compared to the other two datasets generated through the linkage method across the majority of this region. This finding aligns well with our understanding of the area's environmental conditions: the cold climate at high elevations (Fig.4 a), coupled with extensive forest and grassland covers (Fig.4 b), creates an ideal setting for the accumulation of OC in the soil. Therefore, the fine soil property map with a spatial resolution of 90 m can better present the spatial variability of soil properties in related research, which can aid precision agriculture and soil management.

To characterize the spatial pattern differences between CSDLv2 and CSDLv1, Fig. 7 (a, c, e) illustrates the spatial difference maps of OC, sand, and clay predictions in CSDLv2 subtracted by those in CSDLv1 as an example. For OC, the differences are mainly observed in the Tibetan Plateau, Yunnan-Guizhou Plateau, and Northeast Plain, where OC content is higher in CSDLv2 than in CSDLv1. For sand, CSDLv2 shows relatively lower sand content in desert and semi-desert areas (e.g., Taklamakan Desert), while relatively higher sand content is observed in southern coastal regions. For clay, an opposite trend to sand is observed. The possible cause of these differences may be attributed to the linkage method used in developing CSDLv1, which averaged all soil profiles for a given soil type or soil polygon, neglecting local spatial variation in soil properties. Additionally, as shown in Fig. 4, the two datasets derived by DSM technology (i.e., CSDLv2 and SoilGrid 2.0) had similar spatial pattern and higher values than the other two, indicating an underestimation of OC content by the linkage method in this region. The scatter plots in Fig 7 (b, d, f) show the comparison between CSDLv2, CSDLv1, and the observed data. From the bivariate kernel density estimates and correlation coefficients, it is evident that CSDLv2 has a stronger correlation with the observed data. It can also be seen that the scatter points for CSDLv1, based on the linkage method, are more dispersed, whereas the scatter points for CSDLv2, based on DSM technology, are more concentrated. Compared to CSDLv2, CSDLv1 had a significant underestimation of OC and both significant overestimation and underestimation of sand and clay. This may be due to the better fitting ability of DSM technology with available data, but it tends to be more "conservative" in spatial extrapolation, potentially smoothing the properties of certain regions. On the whole, CSDLv2 provides a more accurate estimation of soil properties than CSDLv1, thus it may have significant influences on land surface modeling due to their large differences in spatial distribution. The impact of the new soil dataset instead of the old version and the world soil datasets will need further studies by running a land surface model (Li, et al., 2020).

Based on the experimental results and analysis, compared to CSDLv1, the main advantages of CSDLv2 include the following aspects: First, CSDLv2's spatial resolution is 90 m, an improvement over CSDLv1's 1 km resolution. This addresses the long-standing issue of lacking detailed and accurate soil information and enhances modeling of energy, water, and momentum processes in the land surface model. Second, high-resolution environmental covariates related to soil formation were used with advanced machine learning algorithms, replacing traditional soil transformation rules. In recent years, digital soil mapping technology has made significant progress, particularly with the success of machine learning in large-scale spatial predictions (Poggio et al., 2021). Numerous studies have shown that advanced machine learning models typically have better predictive performance than simpler models (Yan et al., 2020). Third, an RGB soil systems (i.e., red, green and blue) of soil color has been added, resolving the inconvenience of only having the Munsell color system in the first edition dataset. Finally, global validation was conducted using data-splitting and independent samples, and prediction uncertainty was quantitatively provided using QRF, rather than merely offering quality control information. Compared to other related data products: CSDLv2 encompasses more than 20 comprehensive soil physical properties, chemical properties, and fertility, whereas most existing studies focus on mapping one or several fundamental soil properties, lacking comprehensive soil properties data set products (Liang et al., 2019; Chen et al., 2019; Zhou et al., 2019a; Liu et al., 2022a; Liu et al., 2020). For instance, AN serves as an indicator of soil fertility, reflecting the potential release of organic nitrogen and ammonium nitrogen in the soil. AK reflects the potassium available for plant uptake, which is crucial for plant growth and development. The extensive soil information has significant applications across various fields. Additionally, another advantage of CSDLv2 over both CSDLv1 and other related data products is that a large number of soil profile samples from different data sources were collected, enhancing the spatial representativeness of the soil profiles. Sample size is a critical factor affecting model performance (Padarian et al., 2020).

4.2 Potential applications of CSDLv2

The national-scale high-resolution soil property maps developed in this study have significant potential for applications in land surface modeling and Earth system modeling. These models simulate interactions between the land surface, atmosphere, and biosphere, making accurate representation of soil properties essential for improving model performance and predictions. For instance, soil pH is crucial for nutrient solubility, while CEC indicates fertility and nutrient retention capacity in land surface modeling. In biogeochemical process modelling with land surface modeling, OC, TN, and TP are key parameters and prognostic variables. These soil nutrients can be calculated by running models for thousands of years until an equilibrium state is reached, a process known as model "spin-up." (Dai et al., 2019b; Shangguan et al., 2013). However, the non-linear feedbacks in biogeochemical cycles make such "spin-up" time-consuming and less reliable for initializing soil nutrients. Therefore, this dataset can also serve as an important benchmark for initial or calibration variables.

Currently, many soil properties are not yet utilized in land surface model simulations, with only soil texture, OC, gravel and BD being primarily used. However, more soil properties can theoretically be employed as initial variables in Earth system modeling. Each soil property plays an important role in both Earth system modeling and land surface modeling, and although some properties are not yet used, they hold significant potential for future applications. For example, soil albedo is significantly correlated with the Munsell soil color value (hue, value, chroma). In some Earth system models, parameters derived from pedotransfer functions are used directly as inputs rather than being calculated within the models.

Moreover, CSDLv2 offers extensive possibilities for research and applications across various fields, including climate change research and carbon cycling (Chen et al., 2023), as well as precision agriculture (Piikki et al., 2017). Regarding soil pH, for agricultural departments and farmers, fine mapping of soil pH holds significant value in local and field land use planning and management, as different crops exhibit optimal growth in soils with varying pH ranges (Hu et al., 2024). For instance, rice thrives best in soils with pH levels between 6.0 and 7.5, whereas peanuts prefer soils with pH levels between 5.6 and 6.0. Thus, precise soil pH maps provide essential information for agricultural zoning and management. Furthermore, due to the widespread applicability of soil information, CSDLv2 also holds potential applications in numerous other fields.

4.3 Limitations and Outlook

Some advances have been made in this study, but several limitations still need to be addressed in future efforts. First, remote sensing imagery has been used globally for soil property mapping (Guo et al., 2022; Xia and Zhang, 2022). With the advancement of remote sensing technology, more and more high-spatial-resolution free data have become available. For example, Xia and Zhang (2022) found that using high-spatial-resolution GF-2 imagery improved soil property prediction accuracy compared to medium-resolution imagery (e.g., Landsat 8 and Sentinel-2 imagery). Therefore, future digital soil mapping work can focus more on integrating high-resolution remote sensing products, which can enable models to capture the complex statistical relationships between soil properties and the environmental covariates at fine scales (Mulder et al., 2016).

Secondly, soil is a three-dimensional volume with property variability in all three dimensions. In this study, the vertical dimension of soil variability was modeled using spline interpolation. It is noteworthy that smoothing spline interpolation standardizes soil layer data, which is not error-free, but due to the lack of a "true" depth function for each soil profile (vertically dense samples), the standardization error cannot be quantitatively estimated (Liu et al., 2022a). Recent publications have considered observation depth as a covariate (Hengl et al., 2017; Nauman and Duniway, 2019), creating a "3D" model, but some studies indicate that this approach may be overly simplistic or lead to consistency issues in the predicted depth sequences (Ma et al., 2021). This might be true for local datasets, where short-range spatial variability and vertical variability have similar magnitudes (Poggio et al., 2021). Further research is needed to assess the impact of using depth as a covariate on national datasets and models. Additionally, alternatives such as "3D" models or geostatistical models utilizing 3D spatial autocorrelation are worth exploring.

Thirdly, in this study, approximately 150 covariates related to soil properties, topography, climate, biomes, lithology, soil management, and existing soil maps were collected. By removing inter-variable correlations and using recursive feature elimination, approximately 40 optimal variables were selected to map soil properties across the country. However, the original environmental variables with a resolution of 90 meters did not play a significant role in variable selection or importance ranking. Several reasons may explain this. First, many studies have confirmed that soil properties (e.g., soil pH) are highly correlated with lithology (e.g., soil group and parent material) and climatic factors, especially at large scales (Hu et al., 2024; Lu et al., 2023). However, fine and reliable maps of these factors are typically unavailable, especially at large spatial scales. Therefore, when introducing these factors to map soil properties, coarse-resolution raster data (e.g., 1 km) often have to be used (Liu et al., 2022a; Lu et al., 2023). Secondly, in this study, some covariates (e.g., elevation, and slope) with an original resolution of 90 meters are highly correlated with soil properties (e.g., soil pH). However, these factors are also highly correlated with other factors such as mean annual temperature and mean annual precipitation (Guo et al., 2022). These factors were removed by the recursive feature elimination algorithm when selecting the optimal variables because they were highly correlated with the already retained existing variables. This also led to the relatively lower importance of these factors in contributing to the models for soil properties (e.g., soil pH). Therefore, the final maps of soil properties with a 90-meter resolution in this study will be useful for practical decision-making. In future work, introducing fine-resolution environmental covariates is expected to improve mapping accuracy.

Last but not least, this study utilized multi-sources of soil profiles from defferent periods to produce static maps of soil properties, neglecting the time variation of soil properties such as OC. With most soil profiles from the SNSSC, the maps of CSDLv2 majorly represent the status of soil in 1980s. Together with maps based on 2010s soil profiles (Liu et al., 2022a), they could provide new perspectives for studying temporal changes in soil properties. However, more efforts are needed to model the temporal change of soil properties with more time slices, especially for those soil properties which may change in short term, In this aspect, the undergoing Third National Soil Survey of China and other legacy soil profiles should be exploited to map time series of soil properties using spatial-temporal modelling technology.

5 Data and code availability

All resources of Quantile Random Forest model, including training and testing code is publicly available at https://github.com/shgsong/CSDLv2, The soil maps in this study for six depth layers (0-5, 5-15, 15-30, 30-60, 60-100, and 100-200 cm) at 90 m spatial resolution across China are openly accessible: https://doi.org/10.11888/Terre.tpdc.301235 or https://cstr.cn/18406.11.Terre.tpdc.301235 (Shi et al., 2024). To meet the varying spatial resolution requirements of different applications, CSDLv2 offers versions with 90 m, 1 km, and 10 km resolutions. The dataset is provided in raster format, available in both Network Common Data Form 4 (NetCDF4) and GeoTIFF (GTiff) formats.

6 Conclusions

The second version of the high-resolution national soil information grid for China was developed in this study, utilizing a vast number of multi-source legacy soil profile samples and advanced machine learning techniques, as a replacement for the first version dataset. This version includes over 20 soil physical properties, chemical properties and fertility, with prediction maps for each soil property covering six standard depths (0-5, 5-15, 15-30, 30-60, 60-100, and 100-200 cm). By combining Quantile Random Forest with currently available high-resolution environmental covariates, the spatial variations of soil properties across China and at different depths can be effectively predicted. Overall, all the soil property maps performed well, accurately representing the spatial variations of soil properties. Under both data-splitting and independent samples schemes, CSDLv2 generally outperformed other gridded soil property products, including CSDLv1, SoilGrid 2.0, and HWSD 2.0. CSDLv2 exhibited more reasonable spatial patterns and provided more spatial details compared to other soil products. Furthermore, as this dataset is primarily based on legacy soil profiles from the Second National Soil Survey of China, it serves as a valuable complement to maps based on 2010s soil profiles, providing new perspectives for studying temporal changes in soil properties. These prediction maps also contribute to China's input to the GlobalSoilMap project and can be used for various hydrological, ecological analyses, and regional earth system modeling, especially for applications requiring high-resolution soil property maps. Future work can improve soil property mapping by employing advanced deep learning methods and incorporating more observations, particularly in regions with sparse samples like western China.

7 Author contributions

WSG conceived the research and secured funding for the research. GSS and WSG performed the analyses. GSS wrote the initial draft of the manuscript. GSS and WYS conducted the research. WSG and GSS reviewed and edited the paper before submission. All other authors joined the discussion of the research.

8 Competing interests

The authors declare that they have no conflict of interest.

9 Acknowledgements

The authors are grateful to all the data contributors who made it possible to complete this research.

10 Financial support

This work was supported by the Natural Science Foundation of China (under Grants 42375144, 4227515 and 42205149), and Guangdong Major Project of Basic and Applied Basic Research (2021B0301030007).

References

Adhikari, K., Kheir, R. B., Greve, M. B., Bøcher, P. K., Malone, B. P., Minasny, B., McBratney, A. B., and Greve, M. H.: High-Resolution 3-D Mapping of Soil Texture in Denmark, Soil Science Soc of Amer J, 77, 860–876, https://doi.org/10.2136/sssaj2012.0275, 2013.

Arrouays, D., Grundy, M. G., Hartemink, A. E., Hempel, J. W., Heuvelink, G. B. M., Hong, S. Y., Lagacherie, P., Lelyk, G., McBratney, A. B., McKenzie, N. J., Mendonca-Santos, M. d.L., Minasny, B., Montanarella, L., Odeh, I. O. A., Sanchez, P. A., Thompson, J. A., and Zhang, G.-L.: GlobalSoilMap:Toward a Fine-Resolution Global Grid of Soil Properties, in: Advances in Agronomy, vol. 125, Elsevier, 93–134, https://doi.org/10.1016/B978-0-12-800137-0.00003-0, 2014.

Arrouays, D., Savin, I., Leenaars, J., and McBratney, A. B.: GlobalSoilMap-Digital Soil Mapping from Country to Globe: Proceedings of the Global Soil Map 2017 Conference, Moscow, Russia, 2017.

Batjes, N. H.: A global data set of soil pH properties, Tech. Pap.27, Int. Soil Ref. and Int. Soil Ref. And Inf.Cent (ISRIC), Wageningen, Netherlands., 1995.

Batjes, N. H.: Soil parameter estimates for the soil types of the world for use in global and regional modelling (Version 2.1), ISRIC Rep. 2002/02c, Int. Food Policy Res. Inst. (IFPRI) and Int. Soil Ref. Inf. Cent. (ISRIC), Wageningen, Netherlands, 2002.

Batjes, N. H., Ribeiro, E., and van Oostrum, A.: Standardised soil profile data to support global mapping and modelling (WoSIS snapshot 2019), Earth System Science Data, 12, 299–320, https://doi.org/10.5194/essd-12-299-2020, 2020.

Beillouin, D., Demenois, J., Cardinael, R., Berre, D., Corbeels, M., Fallot, A., Boyer, A., and Feder, F.: A global database of land management, land-use change and climate change effects on soil organic carbon, Sci Data, 9, 228, https://doi.org/10.1038/s41597-022-01318-1, 2022.

Bishop, T. F. A., McBratney, A. B., and Laslett, G. M.: Modelling soil attribute depth functions with equal-area quadratic smoothing splines, Geoderma, 91, 27–45, https://doi.org/10.1016/S0016-7061(99)00003-8, 1999.

Breiman, L.: Random Forests, Machine Learning, 45, 5–32, https://doi.org/10. 1023/A:1010933404324, 2001.

Chaney, N. W., Minasny, B., Herman, J. D., Nauman, T. W., Brungard, C. W., Morgan, C. L. S., McBratney, A. B., Wood, E. F., and Yimam, Y.: POLARIS Soil Properties: 30-m Probabilistic Maps of Soil Properties Over the Contiguous United States, Water Resources Research, 55, 2916–2938, https://doi.org/10.1029/2018WR022797, 2019.

Chen, S., Liang, Z., Webster, R., Zhang, G., Zhou, Y., Teng, H., Hu, B., Arrouays, D., and Shi, Z.: A high-resolution map of soil pH in China made by hybrid modelling of sparse soil data and environmental covariates and its implications for pollution, Science of The Total Environment, 655, 273–283, https://doi.org/10.1016/j.scitotenv.2018.11.230, 2019.

Chen, Z., Shuai, Q., Shi, Z., Arrouays, D., Richer-de-Forges, A. C., and Chen, S.: National-scale mapping of soil organic carbon stock in France: New insights and lessons learned by direct and indirect approaches, Soil & Environmental Health, 1, 100049, https://doi.org/10.1016/j.seh.2023.100049, 2023.

Conrad, O., Bechtel, B., Bock, M., Dietrich, H., Fischer, E., Gerlitz, L., Wehberg, J., Wichmann, V., and Böhner, J.: System for Automated Geoscientific Analyses (SAGA) v. 2.1.4, Climate and Earth System Modeling, https://doi.org/10.5194/gmdd-8-2271-2015, 2015.

Crow, W. T., Berg, A. A., Cosh, M. H., Loew, A., Mohanty, B. P., Panciera, R., De Rosnay, P., Ryu, D., and Walker, J. P.: Upscaling sparse ground-based soil moisture observations for the validation of coarse-resolution satellite soil moisture products, Reviews of Geophysics, 50, 2011RG000372, https://doi.org/10.1029/2011RG000372, 2012.

DAAC, O.: MODIS and VIIRS Land Products Global Subsetting and Visualization Tool. In, https://modis.gsfc.nasa.gov, 2018.

Dai, Y., Xin, Q., Wei, N., Zhang, Y., Shangguan, W., Yuan, H., Zhang, S., Liu, S., and Lu, X.: A Global High-Resolution Data Set of Soil Hydraulic and Thermal Properties for Land Surface Modeling, J Adv Model Earth Syst, 11, 2996–3023, https://doi.org/10.1029/2019MS001784, 2019a.

Dai, Y., Shangguan, W., Wei, N., Xin, Q., Yuan, H., Zhang, S., Liu, S., Lu, X., Wang, D., and Yan, F.: A review of the global soil property maps for Earth system models, SOIL, 5, 137–158, https://doi.org/10.5194/soil-5-137-2019, 2019b.

Dinamarca, D. I., Galleguillos, M., Seguel, O., and Faúndez Urbina, C.: CLSoilMaps: A national soil gridded database of physical and hydraulic soil properties for Chile, Sci Data, 10, 630, https://doi.org/10.1038/s41597-023-02536-x, 2023.

Fan, J., Wu, L., Zhang, F., Xiang, Y., and Zheng, J.: Climate change effects on reference crop evapotranspiration across different climatic zones of China during 1956–2015, Journal of Hydrology, 542, 923–937, https://doi.org/10.1016/j.jhydrol.2016.09.060, 2016.

FAO & IIASA: Harmonized World Soil Database version 2.0, FAO; International Institute for Applied Systems Analysis (IIASA), https://doi.org/10.4060/cc3823en, 2023.

Ge, N., Wei, X., Wang, X., Liu, X., Shao, M., Jia, X., Li, X., and Zhang, Q.: Soil texture determines the distribution of aggregate-associated carbon, nitrogen and phosphorous under two contrasting land use types in the Loess Plateau, CATENA, 172, 148–157, https://doi.org/10.1016/j.catena.2018.08.021, 2019.

Gomes, L. C., Faria, R. M., de Souza, E., Veloso, G. V., Schaefer, C. E. G., and Fernandes Filho, E. I.: Modelling and mapping soil organic carbon stocks in Brazil, Geoderma, 340, 337–350, 2019.

Grimm, R. and Behrens, T.: Uncertainty analysis of sample locations within digital soil mapping approaches, Geoderma, 155, 154–163, https://doi.org/10.1016/j.geoderma.2009.05.006, 2010.

Grundy, M. J., Rossel, R. A. V., Searle, R. D., Wilson, P. L., Chen, C., and Gregory, L. J.: Soil and Landscape Grid of Australia, Soil Res., 53, 835, https://doi.org/10.1071/SR15191, 2015.

Guo, J., Wang, K., and Jin, S.: Mapping of Soil pH Based on SVM-RFE Feature Selection Algorithm, Agronomy, 12, 2742, https://doi.org/10.3390/agronomy12112742, 2022.

Gyamerah, S. A., Ngare, P., and Ikpe, D.: Probabilistic forecasting of crop yields via quantile random forest and Epanechnikov Kernel function, Agricultural and Forest Meteorology, 280, 107808, https://doi.org/10.1016/j.agrformet.2019.107808, 2020.

Hengl, T., Heuvelink, G. B. M., Kempen, B., Leenaars, J. G. B., Walsh, M. G., Shepherd, K. D., Sila, A., MacMillan, R. A., Mendes De Jesus, J., Tamene, L., and Tondoh, J. E.: Mapping Soil Properties of Africa at 250 m Resolution: Random Forests Significantly Improve Current Predictions, PLoS ONE, 10, e0125814, https://doi.org/10.1371/journal.pone.0125814, 2015.

Hengl, T., Mendes De Jesus, J., Heuvelink, G. B. M., Ruiperez Gonzalez, M., Kilibarda, M., Blagotić, A., Shangguan, W., Wright, M. N., Geng, X., Bauer-Marschallinger, B., Guevara, M. A., Vargas, R., MacMillan, R. A., Batjes, N. H., Leenaars, J. G. B., Ribeiro, E., Wheeler, I., Mantel, S., and Kempen, B.: SoilGrids250m: Global gridded soil information based on machine learning, PLoS ONE, 12, e0169748, https://doi.org/10.1371/journal.pone.0169748, 2017.

Hengl, T., Miller, M. A. E., Križan, J., Shepherd, K. D., Sila, A., Kilibarda, M., Antonijević, O., Glušica, L., Dobermann, A., Haefele, S. M., McGrath, S. P., Acquah, G. E., Collinson, J., Parente, L., Sheykhmousa, M., Saito, K., Johnson, J.-M., Chamberlin, J., Silatsa, F. B. T., Yemefack, M., Wendt, J., MacMillan, R. A., Wheeler, I., and Crouch, J.: African soil properties and nutrients mapped at 30 m spatial resolution using two-scale ensemble machine learning, Sci Rep, 11, 6130, https://doi.org/10.1038/s41598-021-85639-y, 2021.

Heuvelink, G. B. M., Kros, J., Reinds, G. J., and De Vries, W.: Geostatistical prediction and simulation of European soil property maps, Geoderma Regional, 7, 201–215, https://doi.org/10.1016/j.geodrs.2016.04.002, 2016.

Hu, B., Xie, M., Shi, Z., Li, H., Chen, S., Wang, Z., Zhou, Y., Ni, H., Geng, Y., Zhu, Q., and Zhang, X.: Fine-resolution mapping of cropland topsoil pH of Southern China and its environmental application, Geoderma, 442, 116798, https://doi.org/10.1016/j.geoderma.2024.116798, 2024.

Karger, D. N., Schmatz, D. R., Dettling, G., and Zimmermann, N. E.: High-resolution monthly precipitation and temperature time series from 2006 to 2100, Sci Data, 7, 248, https://doi.org/10.1038/s41597-020-00587-y, 2020.

Koenker, R.: Quantile Regression. Cambridge: Cambridge University Press, https://doi.org/10.1017/CBO9780511754098, 2005.

Krause, P., Boyle, D. P., and Bäse, F.: Comparison of different efficiency criteria for hydrological model assessment, Adv. Geosci., 5, 89–97, https://doi.org/10.5194/adgeo-5-89-2005, 2005.

Lagacherie, P., Arregui, M., and Fages, D.: Evaluating the quality of soil legacy data used as input of digital soil mapping models, European J Soil Science, 75, e13463, https://doi.org/10.1111/ejss.13463, 2024.

Lamichhane, S., Kumar, L., and Wilson, B.: Digital soil mapping algorithms and covariates for soil organic carbon mapping and their implications: A review, Geoderma, 352, 395–413, https://doi.org/10.1016/j.geoderma.2019.05.031, 2019.

Li, Q., Zhang, C., Shangguan, W., Li, L., and Dai, Y.: A novel local-global dependency deep learning model for soil mapping, Geoderma, 438, 116649, https://doi.org/10.1016/j.geoderma.2023.116649, 2023.

Li, W., Wei, N., Huang L., Shangguan W.: Impact of Soil Datasets on the Global Simulation of Land Surface Processes [J]. Climatic and Environmental Research (in Chinese), 25 (5): 555−574. doi: 10.3878/j.issn.1006-9585.2020.20025, 2020.

Liang, Z., Chen, S., Yang, Y., Zhao, R., Shi, Z., and Viscarra Rossel, R. A.: National digital soil map of organic matter in topsoil and its associated uncertainty in 1980's China, Geoderma, 335, 47–56, https://doi.org/10.1016/j.geoderma.2018.08.011, 2019.

Liu, Wu, H., Zhao, Y., Li, D., Yang, J.-L., Song, X., Shi, Z., Zhu, A.-X., and Zhang, G.-L.: Mapping high resolution National Soil Information Grids of China, Science Bulletin, 67, 328–340, https://doi.org/10.1016/j.scib.2021.10.013, 2022a.

Liu, F., Zhang, G.-L., Song, X., Li, D., Zhao, Y., Yang, J., Wu, H., and Yang, F.: High-resolution and three-dimensional mapping of soil texture of China, Geoderma, 361, 114061, https://doi.org/10.1016/j.geoderma.2019.114061, 2020.

Liu, F., Yang, F., Zhao, Y., Zhang, G., and Li, D.: Predicting soil depth in a large and complex area using machine learning and environmental correlations, Journal of Integrative Agriculture, 21, 2422–2434, https://doi.org/10.1016/S2095-3119(21)63692-4, 2022b.

Lu, Q., Tian, S., and Wei, L.: Digital mapping of soil pH and carbonates at the European scale using environmental variables and machine learning, Science of The Total Environment, 856, 159171, https://doi.org/10.1016/j.scitotenv.2022.159171, 2023.

Luo, Y., Ahlström, A., Allison, S. D., Batjes, N. H., Brovkin, V., Carvalhais, N., Chappell, A., Ciais, P., Davidson, E. A., Finzi, A., Georgiou, K., Guenet, B., Hararuk, O., Harden, J. W., He, Y., Hopkins, F., Jiang, L., Koven, C., Jackson, R. B., Jones, C. D., Lara, M. J., Liang, J., McGuire, A. D., Parton, W., Peng, C., Randerson, J. T., Salazar, A., Sierra, C. A., Smith, M. J., Tian, H., Todd-Brown, K. E. O., Torn, M., Van Groenigen, K. J., Wang, Y. P., West, T. O., Wei, Y., Wieder, W. R., Xia, J., Xu, X., Xu, X., and Zhou, T.: Toward more realistic projections of soil carbon dynamics by Earth system models, Global Biogeochemical Cycles, 30, 40–56, https://doi.org/10.1002/2015GB005239, 2016.

Ma, Y., Minasny, B., McBratney, A., Poggio, L., and Fajardo, M.: Predicting soil properties in 3D: Should depth be a covariate?, Geoderma, 383, 114794, https://doi.org/10.1016/j.geoderma.2020.114794, 2021.

Mcbratney, A., Mendonça Santos, M., and Minasny, B.: On Digital Soil Mapping, Geoderma, 117, 3–52, https://doi.org/10.1016/S0016-7061(03)00223-4, 2003.

Meinshausen, N.: Quantile Regression Forests, Journal of Machine Learning Research, 7, 983–999, 2006.

Moreira De Sousa, L., Poggio, L., and Kempen, B.: Comparison of FOSS4G Supported Equal-Area Projections Using Discrete Distortion Indicatrices, IJGI, 8, 351, https://doi.org/10.3390/ijgi8080351, 2019.

Mulder, V. L., Lacoste, M., Richer-de-Forges, A. C., and Arrouays, D.: GlobalSoilMap France: High-resolution spatial modelling the soils of France up to two meter depth, Science of The Total Environment, 573, 1352–1369, https://doi.org/10.1016/j.scitotenv.2016.07.066, 2016.

Nachtergaele, F. O., van Velthuizen, H., Verelst, L., Batjes, N. H., Dijkshoorn, J. A., van Engelen, V. W. P., Fischer, G., Jones, A., Montanarella, L., Petri, M., Prieler, S., Teixeira, E., Wilberg, D., and Shi, X.: Harmonized World Soil Database (version 1.0), , https://soil-modeling.org/resources-links/data-portal/harmonized-world-soil-database, 2012.

National Soil Survey Office: Agricultural Soils in China, China Agricultural Press, Beijing, 1964.

National Soil Survey Office: Chinese Soil Genus Records. vol. 6 China Agriculture Press, Beijing (in Chinese), 1996.

Nauman, T. W. and Duniway, M. C.: Relative prediction intervals reveal larger uncertainty in 3D approaches to predictive digital soil mapping of soil properties with legacy data, Geoderma, 347, 170–184, https://doi.org/10.1016/j.geoderma.2019.03.037, 2019.

Nussbaum, M., Spiess, K., Baltensweiler, A., Grob, U., Keller, A., Greiner, L., Schaepman, M. E., and Papritz, A.: Evaluation of digital soil mapping approaches with large sets of environmental covariates, SOIL, 4, 1–22, https://doi.org/10.5194/soil-4-1-2018, 2018.

Padarian, J., Minasny, B., and McBratney, A. B.: Chile and the Chilean soil grid: A contribution to GlobalSoilMap, Geoderma Regional, 9, 17–28, https://doi.org/10.1016/j.geodrs.2016.12.001, 2017.

Padarian, J., Minasny, B., and McBratney, A. B.: Machine learning and soil sciences: a review aided by machine learning tools, SOIL, 6, 35–52, https://doi.org/10.5194/soil-6-35-2020, 2020.

Piikki, K., Söderström, M., and Stadig, H.: Local adaptation of a national digital soil map for use in precision agriculture, Advances in Animal Biosciences, 8, 430–432, https://doi.org/10.1017/S2040470017000966, 2017.

Poggio, L., De Sousa, L. M., Batjes, N. H., Heuvelink, G. B. M., Kempen, B., Ribeiro, E., and Rossiter, D.: SoilGrids 2.0: producing soil information for the globe with quantified spatial uncertainty, SOIL, 7, 217–240, https://doi.org/10.5194/soil-7-217-2021, 2021.

Qin, D., Ding, Y., and Mu, M. (Eds.): Climate and environmental change in China: 1951 - 2012, Springer, Berlin; Heidelberg, 152 pp., 2016.

Ramcharan, A., Hengl, T., Nauman, T., Brungard, C., Waltman, S., Wills, S., and Thompson, J.: Soil Property and Class Maps of the Conterminous United States at 100-Meter Spatial Resolution, Soil Science Soc of Amer J, 82, 186–201, https://doi.org/10.2136/sssaj2017.04.0122, 2018.

Shangguan, W., Dai, Y., Liu, B., Ye, A., and Yuan, H.: A soil particle-size distribution dataset for regional land and climate modelling in China, Geoderma, 171–172, 85–91, https://doi.org/10.1016/j.geoderma.2011.01.013, 2012.

Shangguan, W., Dai, Y., Liu, B., Zhu, A., Duan, Q., Wu, L., Ji, D., Ye, A., Yuan, H., Zhang, Q., Chen, D., Chen, M., Chu, J., Dou, Y., Guo, J., Li, H., Li, J., Liang, L., Liang, X., Liu, H., Liu, S., Miao, C., and Zhang, Y.: A China data set of soil properties for land surface modeling, J. Adv. Model. Earth Syst., 5, 212–224, https://doi.org/10.1002/jame.20026, 2013.

Shangguan, W., Dai, Y., Duan, Q., Liu, B., and Yuan, H.: A global soil data set for earth system modeling, J. Adv. Model. Earth Syst., 6, 249–263, https://doi.org/10.1002/2013MS000293, 2014.

Shi, G., Shangguan, W.: A China dataset of soil properties for land surface modeling (version 2). National Tibetan Plateau / Third Pole Environment Data Center [data set], https://doi.org/10.11888/Terre.tpdc.301235, https://cstr.cn/18406.11.Terre.tpdc.301235, 2024.

Shi, G., Shangguan, W., Zhang, Y., Li, Q., Wang, C., and Li, L.: Reducing location error of legacy soil profiles leads to improvement in digital soil mapping, Geoderma, 447, 116912, https://doi.org/10.1016/j.geoderma.2024.116912, 2024.

Shiri, J., Keshavarzi, A., Kisi, O., Iturraran-Viveros, U., Bagherzadeh, A., Mousavi, R., and Karimi, S.: Modeling soil cation exchange capacity using soil parameters: Assessing the heuristic models, Computers and Electronics in Agriculture, 135, 242–251, https://doi.org/10.1016/j.compag.2017.02.016, 2017.

Song, X.-D., Wu, H.-Y., Ju, B., Liu, F., Yang, F., Li, D.-C., Zhao, Y.-G., Yang, J.-L., and Zhang, G.-L.: Pedoclimatic zone-based three-dimensional soil organic carbon mapping in China, Geoderma, 363, 114145, https://doi.org/10.1016/j.geoderma.2019.114145, 2020.

Sun, Y., Ma, J., Zhao, W., Qu, Y., Gou, Z., Chen, H., Tian, Y., and Wu, F.: Digital mapping of soil organic carbon density in China using an ensemble model, Environmental Research, 231, 116131, https://doi.org/10.1016/j.envres.2023.116131, 2023.

Thompson, J. A., Kienast-Brown, S., D'Avello, T., Philippe, J., and Brungard, C.: Soils2026 and digital soil mapping – A foundation for the future of soils information in the United States, Geoderma Regional, 22, e00294, https://doi.org/10.1016/j.geodrs.2020.e00294, 2020.

Viscarra Rossel, R. A., Chen, C., Grundy, M. J., Searle, R., Clifford, D., and Campbell, P. H.: The Australian three-dimensional soil grid: Australia's contribution to the GlobalSoilMap project, Soil Res., 53, 845, https://doi.org/10.1071/SR14366, 2015.

Wang, X., Du, P., and Shen, J.: Smoothing splines with varying smoothing parameter, http://arxiv.org/abs/1306.1868, 7 June 2013.

Xia, C. and Zhang, Y.: Comparison of the use of Landsat 8, Sentinel-2, and Gaofen-2 images for mapping soil pH in Dehui, northeastern China, Ecological Informatics, 70, 101705, https://doi.org/10.1016/j.ecoinf.2022.101705, 2022.

Yamashita, N., Ohnuki, Y., Iwahashi, J., and Imaya, A.: National-scale mapping of soil-thickness probability in hilly and mountainous areas of Japan using legacy and modern soil survey, Geoderma, 446, 116896, https://doi.org/10.1016/j.geoderma.2024.116896, 2024.

Yamazaki, D., Ikeshima, D., Sosa, J., Bates, P. D., Allen, G. H., and Pavelsky, T. M.: MERIT Hydro: A High-Resolution Global Hydrography Map Based on Latest Topography Dataset, Water Resources Research, 55, 5053–5073, https://doi.org/10.1029/2019WR024873, 2019.

Yan, F., Shangguan, W., Zhang, J., and Hu, B.: Depth-to-bedrock map of China at a spatial resolution of 100 meters, Sci Data, 7, 2, https://doi.org/10.1038/s41597-019-0345-6, 2020.

Yang, J., Guan, X., Luo, M., and Wang, T.: Cross-system legacy data applied to digital soil mapping: A case study of Second National Soil Survey data in China, Geoderma Regional, 28, e00489, https://doi.org/10.1016/j.geodrs.2022.e00489, 2022.

Zhang, Z., Ding, J., Zhu, C., Wang, J., Ge, X., Li, X., Han, L., Chen, X., and Wang, J.: Historical and future variation of soil organic carbon in China, Geoderma, 436, 116557, https://doi.org/10.1016/j.geoderma.2023.116557, 2023b.

Zhou, Y., Xue, J., Chen, S., Zhou, Y., Liang, Z., Wang, N., and Shi, Z.: Fine-Resolution Mapping of Soil Total Nitrogen across China Based on Weighted Model Averaging, Remote Sensing, 12, 85, https://doi.org/10.3390/rs12010085, 2019a.

Zhou, Y., Hartemink, A. E., Shi, Z., Liang, Z., and Lu, Y.: Land use and climate change effects on soil organic carbon in North and Northeast China, Science of The Total Environment, 647, 1230–1238, https://doi.org/10.1016/j.scitotenv.2018.08.016, 2019b.

Table 1. List of Information of Soil Profiles Data

Soil property	Acronym	Units	Description	Maps
Bulk density	BD	g/cm^3	Bulk density of the fine earth fraction oven dry	Figure S2
Sand	sand	%	Gravimetric percentage of sand (2-0.05mm) in the fine earth fraction of the soil	Figure S3
Silt	silt	%	Gravimetric percentage of silt (0.05-0.02mm) in the fine earth fraction of the soil	Figure S4
Clay	clay	%	Gravimetric percentage of clay (< 0.02mm) in the fine earth fraction of the soil	Figure S5
Rock fragment	gravel	g/100g	Volumetric content of fragments > 2 mm in the whole soil	Figure S6
Porosity	prosity	cm^3/cm^3	Volume fraction of void space (pores) in a material	Figure S7
Wet color	R (Wet)	-	RGB quantified soil color for wet soil	Figure S8
	G (Wet)			Figure S9
	B (Wet)			Figure S10
Dry color	R (Dry)	-	RGB quantified soil color for dry soil	Figure S11
	G (Dry)			Figure S12
	B (Dry)			Figure S13
Wet color	Hue, value, chroma	-	Soil color of wet soil is represented by the Munsell notation with three dimensions: hue, value, and chroma	Figure S14
Dry color	Hue, value, chroma	-	Soil color of dry soil is represented by the Munsell notation with three dimensions: hue, value, and chroma	Figure S15
pH value (H_2O)	pH	-	Negative common logarithm of the activity of hydronium ions (H^+) in water	Figure S16
Soil organic carbon	OC	g/100g	Gravimetric content of organic carbon in the fine earth fraction	Figure S17
Cation exchange capacity	CEC	me/100g	Capacity of the fine earth fraction to hold exchangeable cations	Figure S18
Total nitrogen	TN	g/100g	Total nitrogen in soil, comprising organic, inorganic, and ammonium nitrogen, among other forms	Figure S19
Total phosphorus	TP	g/100g	Total phosphorus in soil includes all phosphorus compounds, both organic and inorganic, irrespective of their plant availability.	Figure S20
Total potassium	TK	g/100g	Total potassium in a soil sample comprises both exchangeable (plant-available) and non-exchangeable forms.	Figure S21
Alkali-hydrolysable nitrogen	AN	mg/kg	Total amount of nitrogen released from soil through alkali treatment (i.e. sodium hydroxide or potassium hydroxide)	Figure S22
Available potassium	AK	mg/kg	Portion of potassium in the soil that is readily accessible for plant uptake	Figure S23
Available phosphorous	AP	mg/kg	Fraction of phosphorus in the soil that is soluble in a chemical extract and readily accessible for plant uptake.	Figure S24

Table 2. Summary of the main high-resolution environmental covariates. For the complete list of soil forming factors, see Table S1.

Factors definitions	Description	Resolution (m)	Source
BDTICM	Depth to bedrock of China	90	http://globalchange.bnu.edu.cn/research/cdtb.jsp
B5/B7	The ratio of Band 5 (near-infrared) to Band 7 (shortwave infrared 2) surface reflectance	90	https://www.usgs.gov/landsat-missions/landsat-collection-2
NDVI	Normalized Difference Vegetation Index	90	Calculated from Landsat 8 Collection 2 Level-2 (LC08C02) on the GEE platform
NDWI	Normalized Difference Water Index	90	Calculated from LC08C02 on the GEE platform
surR	Surface Reflectance	250	https://modis.gsfc.nasa.gov/data/dataprod/mod09.php
EVI	Enhanced Vegetation Index	90	Calculated from LC08C02 on the GEE platform
SAI	Snow Area Index	90	Calculated from LC08C02 on the GEE platform
NPP	Net Primary Productivity	500	https://lpdaac.usgs.gov/products/mod17a3hgfv061/
CanopyHeight	Canopy Height	10	https://doi.org/10.3929/ethz-b-000609802
landcover	Land cover	30	http://www.sciencemag.org/content/342/6160/850
Sentinel2B2/B3/B4/8/9	Band2, 3, 8, 9 from Sentinel2	30	Derived from Sentinel2 on the GEE platform
QA_PIXEL	Landsat 8 Collection 2 Level-2 Pixel Quality Band	90	Derived from LC08C02 on the GEE platform
QA_RADSAT	Radiometric Saturation Quality control	90	Derived from LC08C02 on the GEE platform
SR_B4/B5/B6/B7	Surface Reflectance of Band4, 5, 6, and Band7	90	Derived from LC08C02 on the GEE platform
ST_ATRAN	Atmospheric Transmittance	90	Derived from LC08C02 on the GEE platform
ST_B10	Band 10 Surface Temperature	90	Derived from LC08C02 on the GEE platform
ST_EMSD	Emissivity standard deviation	90	Derived from LC08C02 on the GEE platform
ST_TRAD	Thermal Radiance	90	Derived from LC08C02 on the GEE platform
ST_URAD	Downwelled Radiance	90	Derived from LC08C02 on the GEE platform
DEM	Land surface elevation	90	https://hydro.iis.u-tokyo.ac.jp/~yamadai/MERIT_DEM/
slope	Terrain slope	90	Derived from DEM
Land use	Land use type	30	https://www.resdc.cn/DOI/DOL.aspx?DOIID=54
RTMUSG15	Rock type	250	https://doi.pangaea.de/10.1594/PANGAEA.788537

Table 3. Predictive performance of selected soil properties in CSDLv2, CSDLv1, SoilGrids 2.0, and HWSD 2.0. Twenty repeats of 10-fold cross-validation with testing soil profiles for CSDLv2, and validation using all soil profiles for other datasets. Refer to Table S4 for the complete predictive performance of the soil properties considered. See Table 1 for the abbreviations and units of the soil properties interested.

Property	Depth interval	CSDLv2			CSDLv1			SoilGrids 2.0			HWSD 2.0		
		MEC	RMSE	ME	MEC	RMSE	ME	MEC	RMSE	ME	MEC	RMSE	ME
pH	0-5	0.69	0.70	0.00	0.48	0.92	-0.03	0.60	0.79	-0.15	0.35	1.03	-0.28
	5-15	0.70	0.68	0.00	0.50	0.90	-0.02	0.61	0.77	-0.12	0.36	1.02	-0.13
	15-30	0.70	0.68	0.00	0.26	1.21	-0.41	0.60	0.77	-0.16	0.38	1.03	-0.15
	30-60	0.68	0.70	-0.00	0.43	0.94	-0.04	0.59	0.78	-0.15	0.38	1.02	-0.17
	60-100	0.68	0.70	0.00	0.44	0.94	0.04	0.59	0.78	-0.14	0.39	1.01	-0.18
	100-200	0.75	0.60	0.00	0.53	0.84	-0.05	0.63	0.70	-0.09	0.52	0.87	-0.08
sand	0-5	0.67	12.15	0.05	0.19	22.19	-2.24	0.60	13.08	-1.84	0.20	21.84	2.38
	5-15	0.71	11.23	0.06	0.18	21.90	-2.28	0.62	11.87	-1.93	0.19	21.43	1.40
	15-30	0.71	11.41	0.05	0.15	22.58	-1.67	0.62	11.85	-1.71	0.14	21.89	2.63
	30-60	0.69	12.16	0.06	0.13	23.26	-1.31	0.59	12.68	-1.80	0.12	22.57	3.68
	60-100	0.68	12.85	0.04	0.11	23.22	-1.30	0.51	13.53	-1.94	0.10	23.45	4.03
	100-200	0.64	13.72	0.02	0.10	24.22	-1.42	0.49	14.59	-1.88	0.09	24.11	3.98
silt	0-5	0.61	9.81	0.02	0.11	16.78	2.02	0.55	10.54	-0.58	0.10	17.38	-4.44
	5-15	0.65	8.99	-0.00	0.13	16.31	2.29	0.58	9.22	-0.33	0.10	16.90	-5.55
	15-30	0.67	8.76	0.00	0.13	16.29	2.12	0.60	9.02	-0.51	0.09	17.30	-6.46
	30-60	0.63	9.49	0.00	0.11	16.55	1.76	0.57	9.68	-0.41	0.10	17.53	-6.36
	60-100	0.62	10.08	0.00	0.10	17.05	1.49	0.55	10.34	-0.33	0.10	18.07	-6.15
	100-200	0.64	10.60	0.01	0.09	17.94	0.70	0.54	11.25	-0.99	0.11	19.14	-5.15
clay	0-5	0.63	6.74	0.01	0.12	11.23	0.21	0.52	7.60	2.49	0.12	11.14	2.06
	5-15	0.67	6.50	0.01	0.09	11.28	0.03	0.58	7.18	2.36	0.09	11.89	4.23
	15-30	0.68	6.83	0.01	0.10	11.83	0.61	0.60	7.40	2.28	0.09	12.78	3.95
	30-60	0.68	7.36	0.02	0.09	12.78	0.14	0.61	7.89	2.22	0.13	13.20	2.70
	60-100	0.68	7.79	0.02	0.07	13.43	-0.28	0.61	8.33	2.21	0.12	13.65	1.97
	100-200	0.63	7.96	0.03	0.06	13.00	0.86	0.55	8.67	2.74	0.12	13.06	0.91
BD	0-5	0.62	0.12	0.00	0.12	0.20	0.01	0.53	0.13	0.01	0.02	0.27	0.15
	5-15	0.63	0.11	0.00	0.15	0.19	0.01	0.57	0.12	0.01	0.01	0.29	0.18
	15-30	0.60	0.11	-0.00	0.11	0.19	0.01	0.54	0.13	0.01	0.01	0.27	0.12
	30-60	0.55	0.12	-0.00	0.10	0.19	-0.01	0.53	0.13	-0.00	0.01	0.24	0.10
	60-100	0.57	0.12	-0.00	0.10	0.19	-0.01	0.51	0.13	-0.01	0.02	0.24	0.07
	100-200	0.47	0.13	0.00	0.05	0.22	0.02	0.42	0.13	-0.01	0.02	0.24	0.07

https://doi.org/10.5194/essd-2024-299
Preprint. Discussion started: 29 August 2024

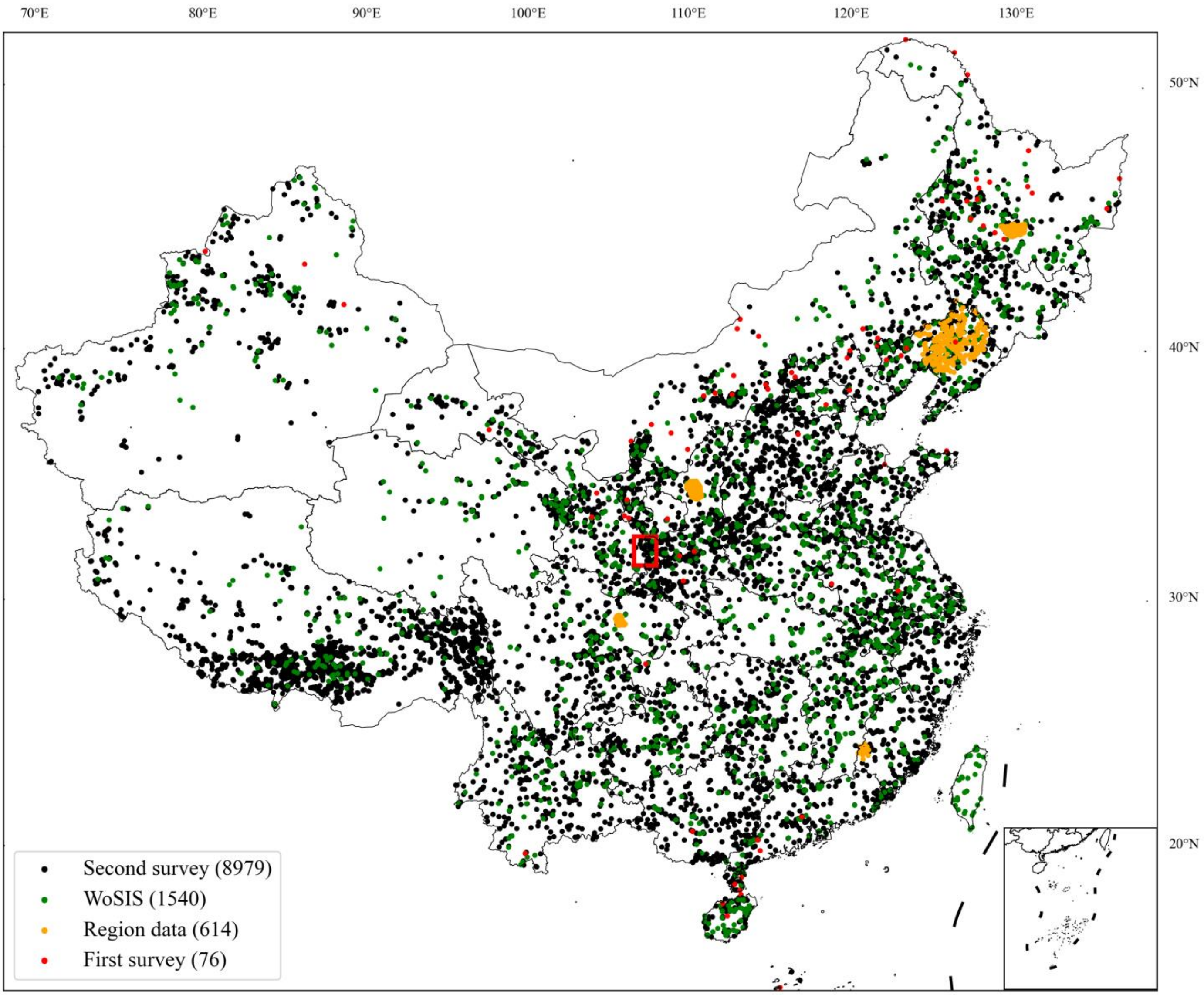

810 **Figure 1. Spatial distribution of the 11,209 soil profiles collected from various data sources in this study: black dots indicate the Second National Soil Survey of China (Second survey), green dots correspond to World Soil Information Service (WoSIS), orange dots denote regional data, and red dots represent the First National Soil Survey of China (First survey). The red window indicates the area selected for visualizing the spatial patterns of soil properties.**

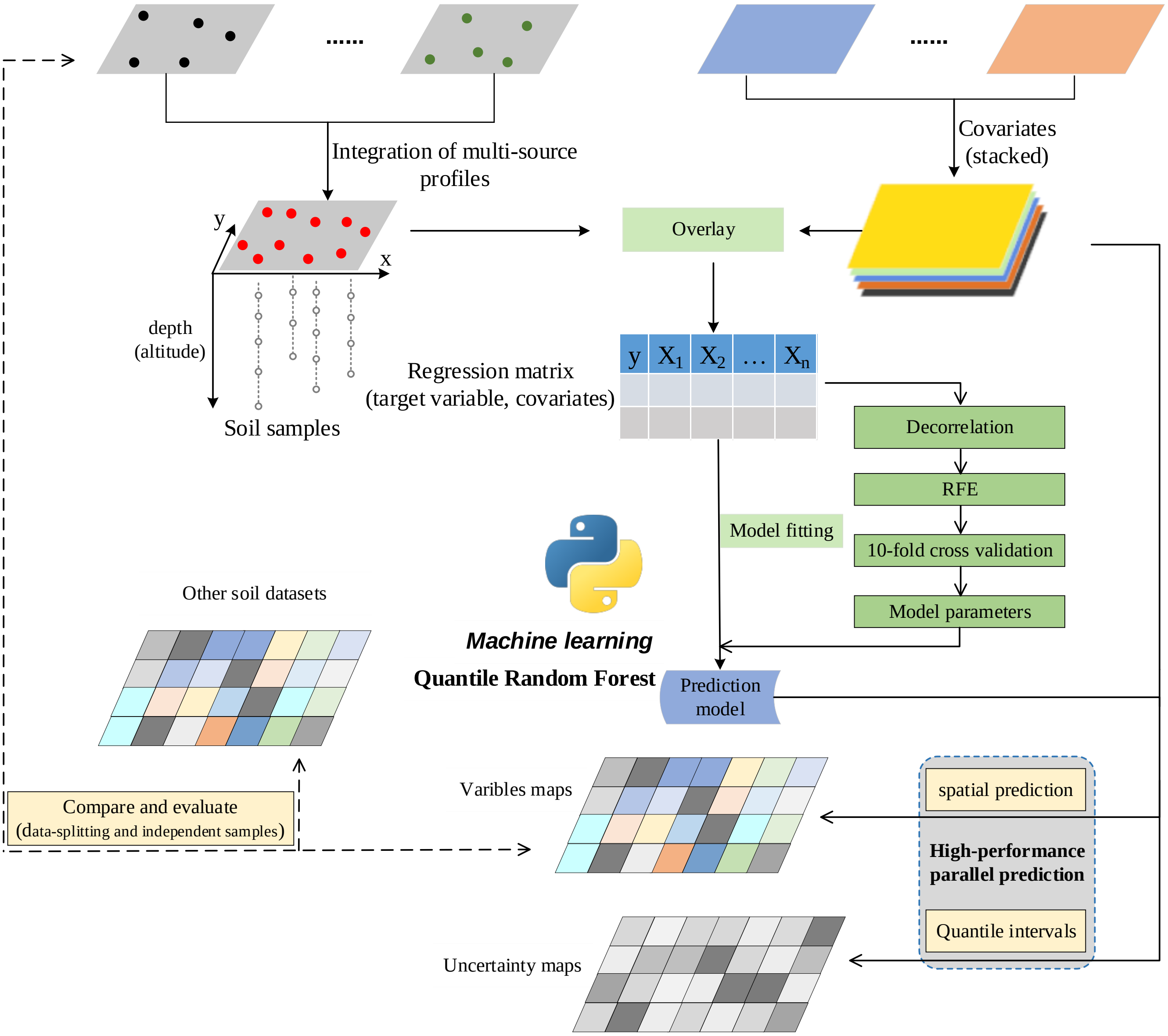

815 **Figure 2. The statistical framework for developing national-scale soil properties mapping in this study.**

https://doi.org/10.5194/essd-2024-299
Preprint. Discussion started: 29 August 2024

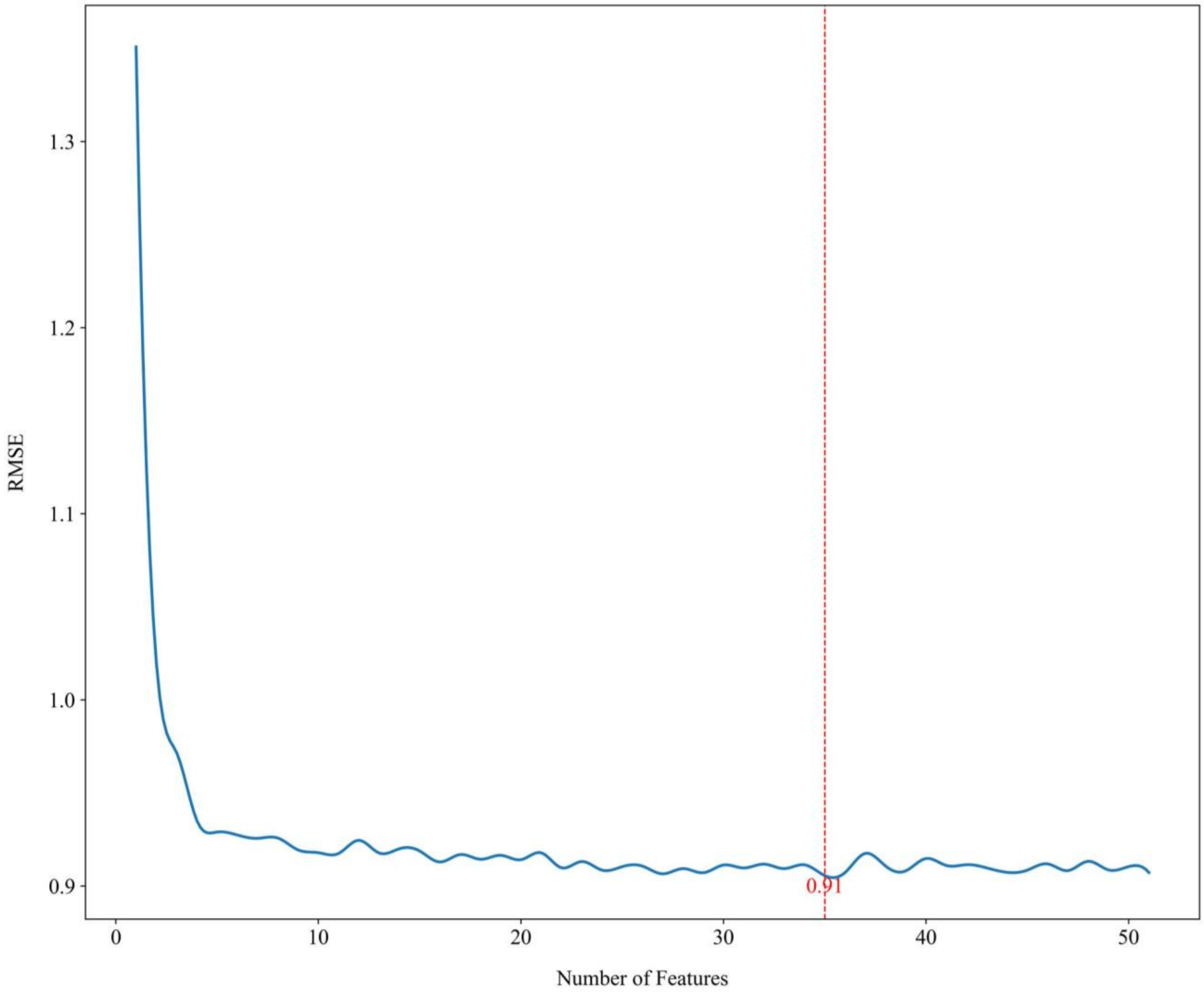

Figure 3. Example of the loss function (RMSE) used in the Recursive Feature Elimination (RFE) step of covariates' selection for surface (0-5 cm) soil organic carbon.

https://doi.org/10.5194/essd-2024-299
Preprint. Discussion started: 29 August 2024

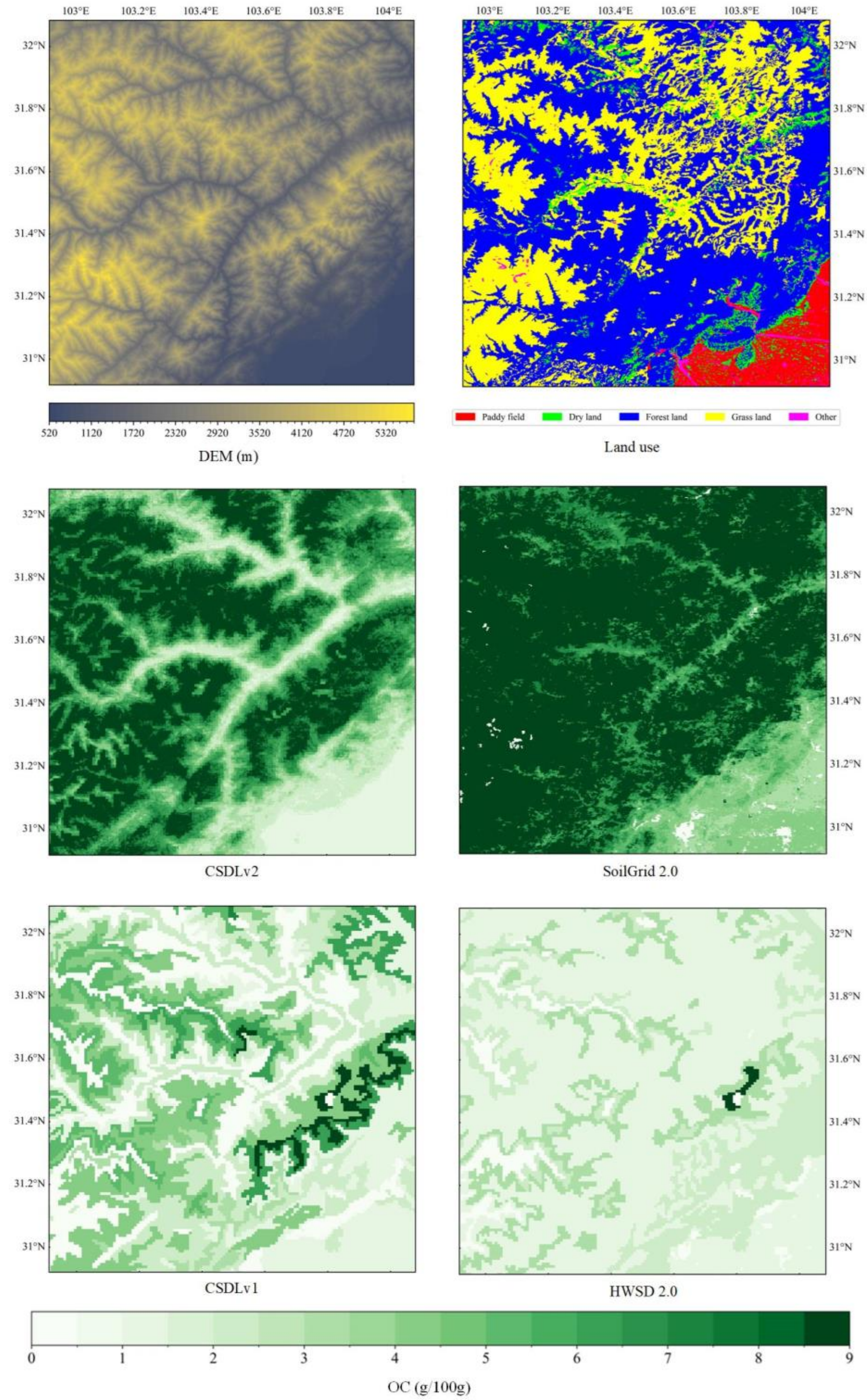

820 **Figure 4. Surface (0-5cm) soil organic carbon (OC) maps derived from our predictions (CSDLv2), SoilGrid 2.0, CSDLv1, and HWSD 2.0, respectively, in a selected area (102.92°-104.08°E and 30.92°-32.08°N) located in Sichuan Province. This selected area corresponds to the red window shown in Figure 1. The spatial resolutions are 90 m for CSDLv2, 250 m for SoilGrid 2.0, and 1 km for both CSDLv1 and HWSD 2.0.**

https://doi.org/10.5194/essd-2024-299
Preprint. Discussion started: 29 August 2024

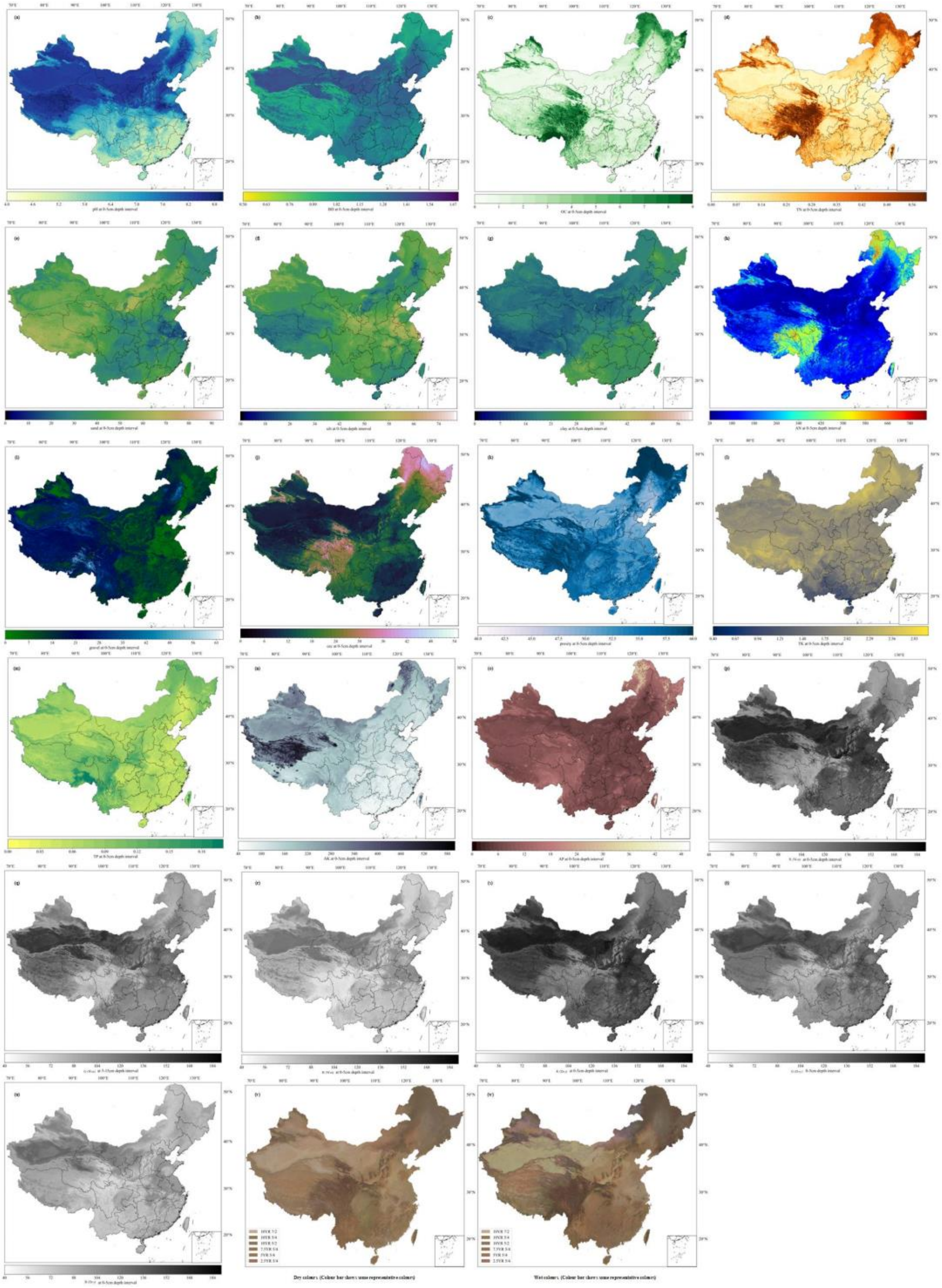

825 **Figure 5. The predicted maps of soil properties considered at 0-5 cm depth interval. (a) pH (H_2O); (b) bulk density (BD); (c) soil organic carbon (OC); (d) total nitrogen (TN); (e,f,g) soil texture(sand, silt ,clay); (h) Alkali-hydrolysable N (AN); (i) Rock fragment (gravel); (j) cation exchange capacity (CEC); (k) porosity; (l) total potassium (TK); (m) total phosphorus (TP); (n) Available potassium (AK); (o) Available phosphorous (AP); (p,q,r) Wet color (R, G, B); (s,t,u) Dry color (R, G, B). (v) and (w) represent the dry and wet colors in the Munsell color system, respectively. See Figures S2-S24 in the appendix for the predicted maps of soil properties at all depth intervals.**

https://doi.org/10.5194/essd-2024-299
Preprint. Discussion started: 29 August 2024

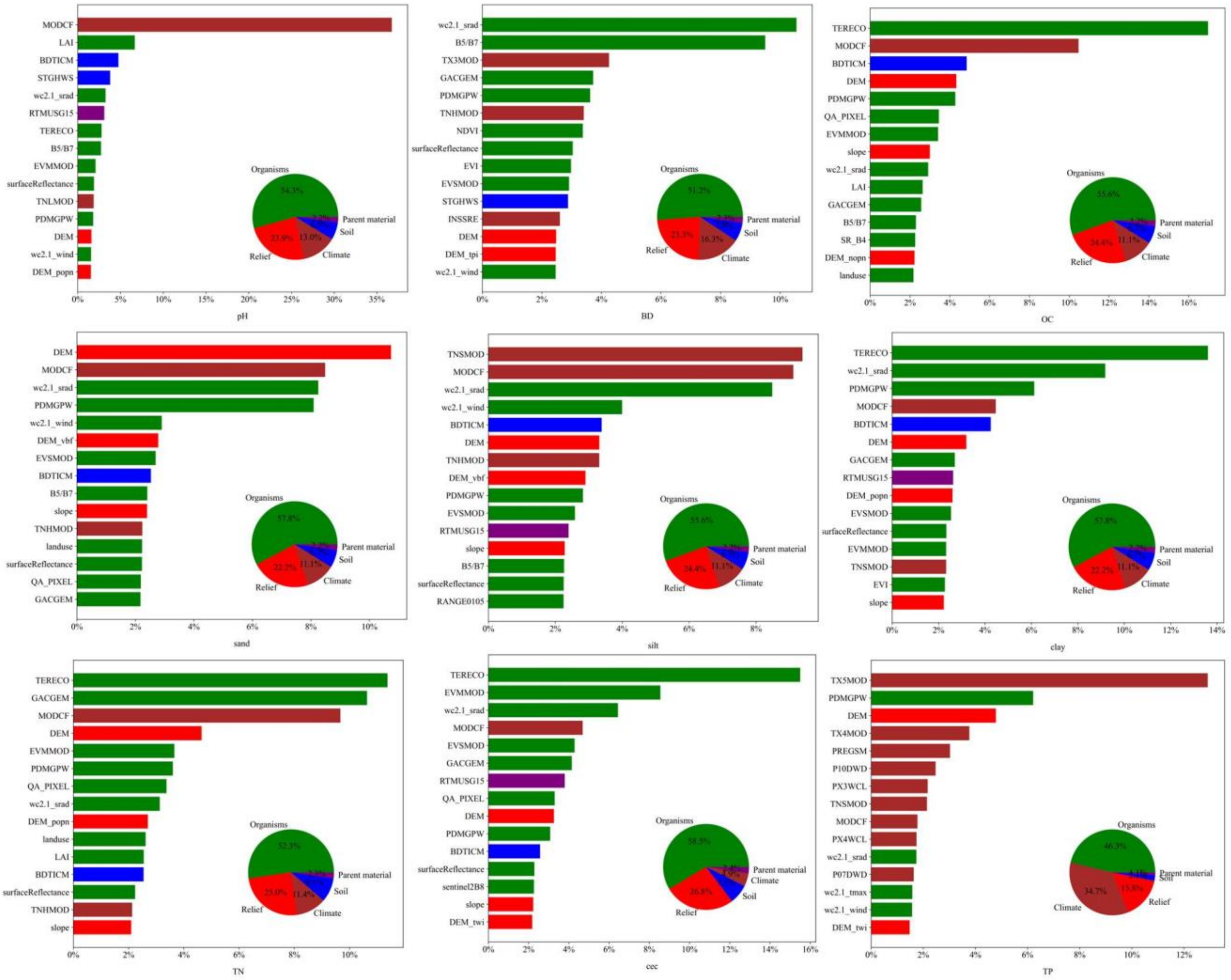

Figure 6. Relative importance of predictors for the Quantile Regression Forest model in the spatial predictions of soil pH, bulk density (BD), soil organic carbon (OC), soil texture (sand, silt, clay), total nitrogen (TN), cation exchange capacity (CEC), and total phosphorus (TP) at the surface layer (0-5 cm). For other surface soil properties interested, including alkali-hydrolysable nitrogen (AN), rock fragment (gravel), porosity, total potassium (TK), available potassium (AP), available phosphorus (AP), wet color (R, G, B), and dry color (R, G, B), see Figure S26. Refer to Table S1 in the appendix for abbreviations of the environmental covariates.

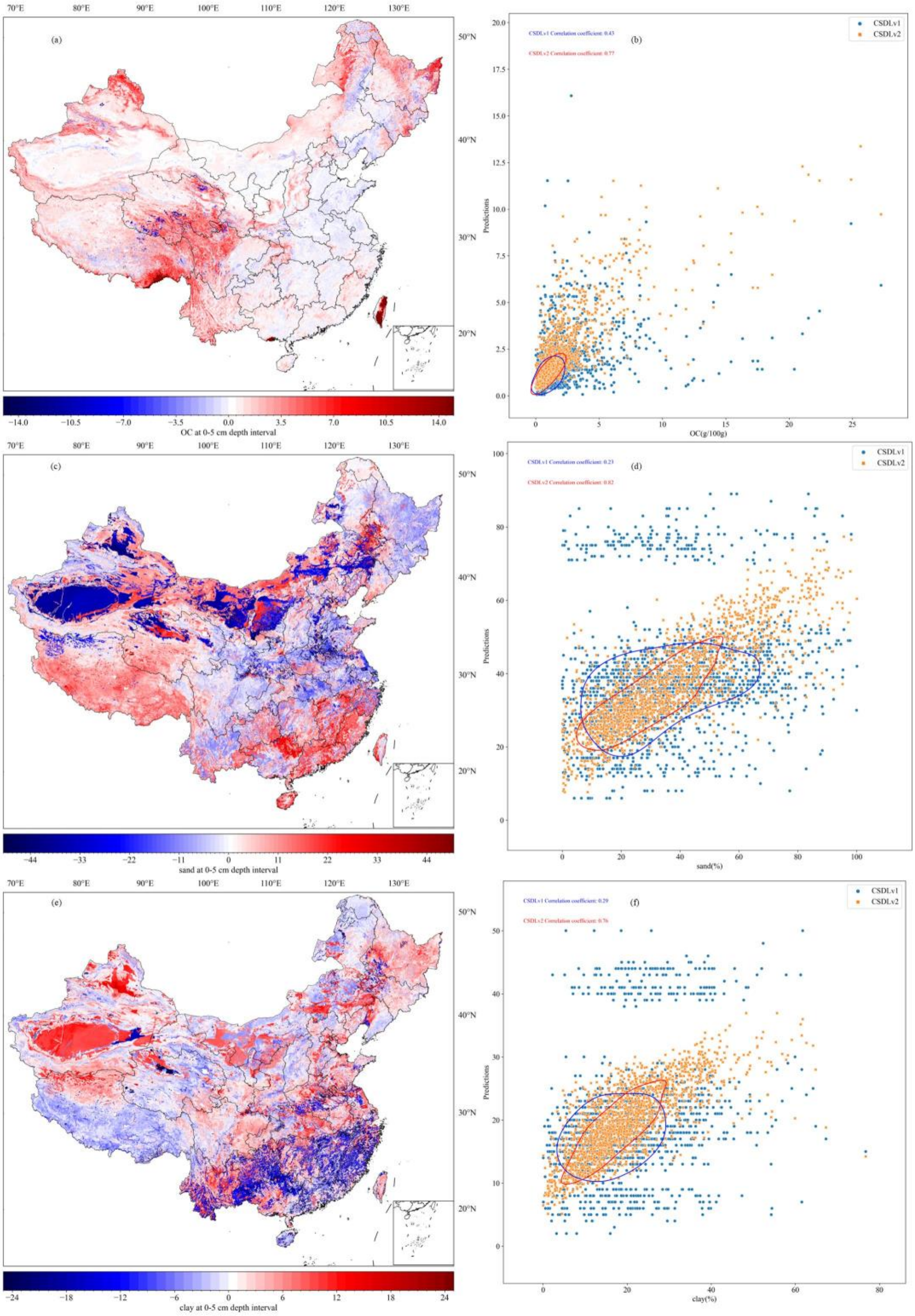

Figure 7. Differences in predicted maps of soil organic carbon (a), sand (c), and clay (e) between CSDLv2 and CSDLv1 at the 0-5 cm depth interval and the corresponding scatter plots (b, d, f) indicating how well the predictions of CSDLv2 and CSDLv1 match the observations. 840 The red and blue circles are bivariate kernel density estimates.